


**ESA Cloud\_cci+**  
**Product Validation and Intercomparison Report -**  
**Demonstrator data v3**



Issue 3 Revision 0


20.11.2023

Deliverable No.: D-4.1  
ESRIN/Contract No.: 4000128637/20/I-NB  
Science lead: Dr. Martin Stengel  
Deutscher Wetterdienst  
martin.stengel@dwd.de  
Technical Officer: Michael Eisinger  
European Space Agency  
Michael.Eisinger@esa.int

	<b>Doc:</b>		Cloud_cci+_D4.1_PVIR_v3.0.docx		
	<b>Date:</b>		20.11.2023		
	<b>Issue:</b>	3	<b>Revision:</b>	0	Page 2


## Document Change Record

Document, Version	Date	Changes	Originator
v2.0_submitted	02/08/2022	Initial version, heritage from D4.1_PVIR_v1.1, now evaluating v2 demonstrator data	D. Philipp M. Stengel E. Carboni
v2.0	24/11/2022	approved version	D. Philipp M. Stengel E. Carboni
v3.0_submitted	07.07.2023	Updated version, including validation results for v3 data - replacing the v2 results	D. Philipp M. Stengel E. Carboni
v3.0	20.11.2023	Final and approved version	M. Stengel

	Doc:		Cloud_cci+_D4.1_PVIR_v3.0.docx		
	Date:		20.11.2023		
	Issue:	3	Revision:	0	Page 3

## Contents

1	INTRODUCTION.....	6
1.1	The ESA Cloud_cci+ project .....	6
1.1.1	Cloud_cci+ Phase I.....	6
1.2	Cloud_cci cloud and radiative flux products .....	6
1.3	Validation strategy in this report .....	9
1.3.1	Evaluation measures .....	9
1.3.2	Datasets used for evaluation.....	10
2	EVALUATION OF SEVIRI V3 DATA .....	12
2.1	Level-2 data.....	12
2.1.1	Validation of SEVIRI Level-2 CMA, CPH and CTH with CALIOP.....	12
2.1.2	Validation of SEVIRI Level-2 IWP with DARDAR.....	15
2.1.3	Validation of SEVIRI Level-2 LWP with AMSR2 .....	17
2.2	Level-3 data.....	19
2.2.1	Validation of SEVIRI Level-3C CFC with SYNOP data.....	19
2.2.2	Validation of SEVIRI Level-3 radiative fluxes with CERES and BSRN.....	19
2.2.3	Intercomparison against CM-SAF CLAAS-3 .....	24
3	EVALUATION OF SLSTR V3 DATA.....	28
3.1	Level-2 data.....	28
3.1.1	Validation of SLSTR Level-2 LWP with AMSR2 .....	28
3.2	Level-3 data.....	29
3.2.1	Comparisons with SEVIRI data .....	29
3.2.2	Comparison with MODIS collection 6.....	31
3.2.3	Validation of SLSTR Level-3 radiative fluxes with CERES and BSRN .....	39
4	SUMMARY .....	46
5	DEFINITIONS, ACRONYMS, ABBREVIATIONS.....	47
6	REFERENCES .....	49
	ANNEX A - DATASETS FOR COMPARISONS WITH CLOUD_CCI PRODUCTS .....	51
A.1	CALIPSO-CALIOP .....	51

	<b>Doc:</b>		Cloud_cci+_D4.1_PVIR_v3.0.docx		
	<b>Date:</b>		20.11.2023		
	<b>Issue:</b>	3	<b>Revision:</b>	0	Page 4

A.2 AMSR2 .....52


A.3 DARDAR .....54

A.4 BSRN: Baseline Surface Radiation Network.....55

A.5 SYNOP: manual cloud observations from surface stations .....56

A.6 CERES: Cloud and the Earth’s Radiant Energy System .....57

A.7 CLAAS-3: CLOUD property dAtAset using SEVIRI .....58

	<b>Doc:</b>		Cloud_cci+_D4.1_PVIR_v3.0.docx		
	<b>Date:</b>		20.11.2023		
	<b>Issue:</b>	3	<b>Revision:</b>	0	Page 5

### Scope of this document

This document is the Product Validation and Intercomparison Report (PVIR) for ESA Cloud\_cci+ Phase I. It covers the validation results for the generated version 3 demonstrator data sets for SEVIRI and SLSTR covering all months in 2019.

# 1 Introduction

## 1.1 The ESA Cloud\_cci+ project

The Cloud\_cci+ project contributes to and improves on the successful efforts of Cloud\_cci: the development, validation and application of novel cloud property data sets maximising the use of ESA and other European EO mission data and targeting the GCOS requirements for the Cloud ECV. The current Cloud\_cci+ project phase I was kicked off in March 2020.

### 1.1.1 Cloud\_cci+ Phase I

The goal of the ESA Cloud\_cci+ is the improvement of retrieval algorithms and processing concepts and implementations, and the development of two demonstrator data sets based on measurements from the Spinning Enhanced Visible and Infrared Imager (SEVIRI) and from the Sea and Land Surface Temperature Radiometer (SLSTR). The processing systems will have the potential to be used for a sustained data production in operational entities, for instance the EUMETSAT SAF network and the Copernicus Climate Change Service, after the current R&D under the ESA CCI programme has been completed.

Focus of the further CC4CL developments will be on:

- Enhance the CC4CL capabilities wrt. utilizing the advanced spectral information available from SEVIRI and SLSTR compared to the AVHRR-heritage.
- Improvement of cloud detection over snow and ice surfaces (e.g. in polar regions), in mountainous regions and in the presence of optically thin cirrus clouds
- Improvement of cloud phase determination and the detection of multi-layer cloud situations as knowledge of both aspects significantly impacts the subsequent retrieval of cloud properties
- Improvement of the uncertainty characterizations

A full list of planned and carried out developments is given (and regularly updated) in the Algorithm Development Plan (ADPv3.0). The cloud products retrieved from SEVIRI and SLSTR remain the same compared to previous datasets and are outlined in the next subsection. Examples are shown in Figure 1-1.

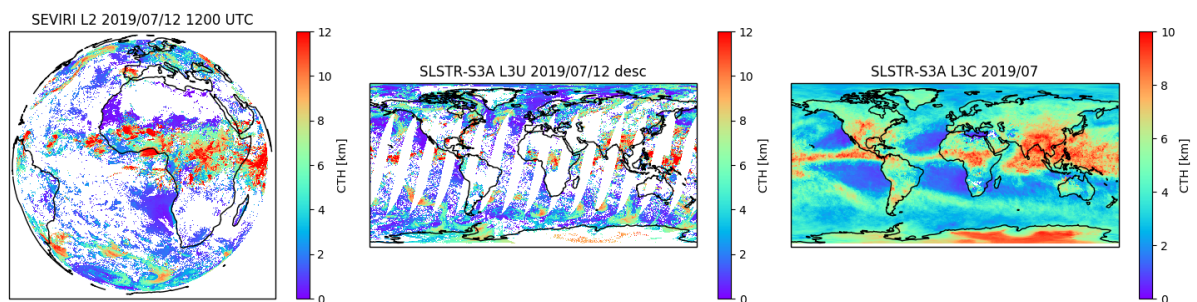


**Figure 1-1** Examples of Level-2 cloud top height fields from SEVIRI (left) and SLSTR-S3a (middle). Right panel depicts an example monthly mean cloud top height field from SLSTR-S3a.

## 1.2 Cloud\_cci cloud and radiative flux products

The cloud properties derived on satellite pixel level of each utilized sensor are listed in Table 1-1. Primarily retrieved cloud properties are CMA/CFC, CPH, CTP, COT and CER. The properties CLA, LWP, IWP are determined from retrieved COT and CER in a post processing step. The same applies to CTH and CTT, which are inferred from the retrieved CTP. Radiative fluxes properties are calculated using radiative transfer calculation (requiring ERA5 data) ingesting the retrieved cloud properties.

Based on the pixel level retrievals the data is further processed into different processing levels as summarized in Table 1-2. Level-3U denotes a global composite on a global Latitude-Longitude grid (of 0.05° resolution) onto which the Level-2 data is sampled. Level-3C products are also defined on Latitude-Longitude grid (0.5° resolution) onto which the properties are averaged and their frequency collected (histograms). Further separation of cloud properties in Level-3C in e.g. day/night, liquid/ice, were made wherever suitable (see Table 1-3). The reader is referred to [ATBDv9.0](#) for more details on Level-3U and Level-3C generation)

**Table 1-1** List of generated cloud properties. CMA/CFC and CPH are derived in a pre-processing step using Artificial Neural Networks. In the next step, COT, CER and CTP are retrieved simultaneously by fitting a physically consistent cloud/atmosphere/surface model to the satellite observations using optimal estimation (OE). Moreover, LWP and IWP are obtained from COT and CER. In addition, spectral cloud albedo (CLA) for two visible channels are derived. In a post-processing step, derived cloud properties and ERA-Interim information are used to determine radiative broadband fluxes. The Photosynthetically active radiation (PAR) is no standard output.

Variable	Abbrev.	Definition
Cloud mask / Cloud fraction	CMA/ CFC	A binary cloud mask per pixel (L2, L3U) and therefrom derived monthly total cloud fractional coverage (L3C) and separation into 3 vertical classes (high, mid-level, low clouds) following ISCCP classification ( <a href="#">Rossow and Schiffer, 1999</a> ).
Cloud phase	CPH	The thermodynamic phase of the retrieved cloud (binary: liquid or ice; in L2, L3U) and the therefrom derived monthly liquid cloud fraction (L3C).
Cloud optical thickness	COT	The line integral of the absorption coefficient and the scattering coefficient (at 0.55µm wavelength) along the vertical in cloudy pixels.
Cloud effective radius	CER	The area-weighted radius of the cloud drop and crystal particles, respectively.
Cloud top pressure/ height/ temperature	CTP/ CTH/ CTT	The air pressure [hPa] /height [m] /temperature [K] of the uppermost cloud layer that could be identified by the retrieval system.
Cloud liquid water path/ Ice water path	LWP/ IWP	The vertical integrated liquid/ice water content of existing cloud layers; derived from CER and COT. LWP and IWP together represent the cloud water path (CWP)
Joint cloud property histogram	JCH	This product is a spatially resolved two-dimensional histogram of combinations of COT and CTP for each spatial grid box.
Spectral cloud albedo	CLA	The blacksky cloud albedo derived for channel 1 (0.67 µm) and 2 (0.87 µm), respectively (experimental product)
Cloud effective emissivity	CEE	cloud radiative thickness in the infrared typically referred to as the “effective emissivity”
Top of atmosphere upwards/downwards flux	TOA	Shortwave (SW) and longwave (LW) fluxes at the Top of the atmosphere, upwelling and downwelling
Top of atmosphere upwards/downwards flux - clear-sky	TOA <sub>clear</sub>	Shortwave (SW) and longwave (LW) fluxes at the Top of the atmosphere, upwelling and downwelling - for clear sky conditions
Bottom of atmosphere (surface) upwards/downwards flux	BOA	Shortwave (SW) and longwave (LW) fluxes at the Bottom of the atmosphere, upwelling and downwelling
Bottom of atmosphere (surface) upwards/downwards flux - clear-sky	BOA <sub>clear</sub>	Shortwave (SW) and longwave (LW) fluxes at the Bottom of the atmosphere, upwelling and downwelling - for clear sky conditions
Photosynthetically active radiation	PAR	Bottom of atmosphere incoming shortwave radiation in the spectral range between 400 and 700nm

**Table 1-2 Processing levels of Cloud\_cci data products. Level-3U and Level-3C are each directly derived from Level-2.**

Processing level	Spatial resolution	Description
<b>Level-2 (L2)</b>	SLSTR: 1km SEVIRI: 3-5 km	Retrieved cloud variables at satellite sensor pixel level, thus with the same resolution and location as the sensor measurements (Level-1)
<b>Level-3U* (L3U)</b>	Latitude-Longitude grid at 0.05° res.	Cloud properties of Level-2 orbits projected onto a global space grid without combining any observations of overlapping orbits. Only subsampling is done. Common notation for this processing level is also L2b. Temporal coverage is 24 hours (0-23:59 UTC).
<b>Level-3C (L3C)</b>	Latitude-Longitude grid at 0.5° res.	Cloud properties of Level-2 orbits of one single sensor combined (averaged / sampled for histograms) on a global space grid. Temporal coverage of this product is 1 month.

\* Level-3U data are only provided for SLSTR and not for SEVIRI products

**Table 1-3 Cloud\_cci product features incl. day and night separation, liquid water and ice as well as histogram representation. Level-3U refers to the un-averaged, pixel-based cloud retrievals sampled onto a global Latitude-Longitude (lat/lon) grid. <sup>1</sup>CMA in Level-2 and Level-3U is a binary cloud mask. All products listed exist in each dataset listed above.**

	Level 2 swath based 1km/5km	Level-3U* daily sampled global 0.05° lat/lon grid	Level-3C monthly averages global 0.5° lat/lon grid	Level-3C monthly histograms global 0.5° lat/lon grid
<b>CMA/CFC</b>	✓ as CMA <sup>1</sup>	✓ as CMA <sup>1</sup>	✓ day/night/high/mid/low	-
<b>CTP, CTH, CTT</b>	✓	✓	✓	✓ liquid/ice
<b>CPH</b>	✓	✓	✓ day/night	-
<b>COT</b>	✓	✓	✓ liquid/ice	✓ liquid/ice
<b>CER</b>	✓	✓	✓ liquid/ice	✓ liquid/ice
<b>LWP</b>	✓ as CWP	✓ as CWP	✓	✓ as CWP
<b>IWP</b>			✓	
<b>CLA</b>	✓ 0.6/0.8µm	✓ 0.6/0.8µm	✓ 0.6/0.8µm	✓ 0.6/0.8µm/liquid/ice
<b>JCH</b>	-	-	-	✓ liquid/ice
<b>TOA<sub>up,dn,sw,lw</sub></b>	✓	✓	✓	-
<b>BOA<sub>up,dn,sw,lw</sub>, PAR</b>	✓	✓	✓	-

\* Level-3U data are only provided for SLSTR and not for SEVIRI products



### 1.3 Validation strategy in this report

#### 1.3.1 Evaluation measures

For geophysical quantities at Level-2, such as cloud top height, and for averaged products (Level-3C), we use the bias, i.e. mean difference between Cloud\_cci and reference data as the metric for accuracy. In addition, the bias corrected root mean squared error (bc-RMSE) is used to express the precision of Cloud\_cci products compared to the reference data.

**Bias (accuracy):** Mean bias between Cloud\_cci and reference data.

Calculated as  $\frac{1}{N} \sum_{i=1}^N (x_i - y_i)$  where N is the sample size,  $x_i$  the Cloud\_cci observation and  $y_i$  the reference observation.

**bc-RMSE (precision):**

Bias corrected root mean squared error to express the precision of Cloud\_cci compared to a reference data record.

Calculated as  $\sqrt{\frac{1}{N} \sum_{i=1}^N (x_i - \bar{y})^2}$  where N is the sample size,  $x_i$  the Cloud\_cci observation and  $\bar{y}$  the mean of the reference data.

In case of binary Level-2 data with only two possible events, e.g. cloud mask (clear or cloudy) and cloud phase (liquid or ice), we use the scores of Table 1-5 which can be derived from the contingency table (Table 1-4).

**Table 1-4: Contingency table for the 2x2 problem.**  $n_{ij}$  is the number of cases where Cloud\_cci reports event and the reference reports event  $j$ . For example event 1 may be cloudy and event 0 may be clear.

	Reference reports 1	Reference reports 0
Cloud_cci+ reports 1	$n_{11}$	$n_{12}$
Cloud_cci+ reports 0	$n_{21}$	$n_{22}$

**Table 1-5: Scores for evaluation of binary variables as cloud mask or cloud phase.** Input to the formulas are the values from the 2x2 contingency table (Table 1-4).

Score	Description	Calculation
Hitrate	The total fraction of all correct Cloud_cci reports relative to all reference reports.	$\frac{n_{11} + n_{22}}{n_{11} + n_{12} + n_{21} + n_{22}}$ $\in [0,1], 1 \text{ is best}$
Probability Of Detection (POD)	The fraction of correct Cloud_cci reports of a particular category relative to all reference reports of this category.	POD for event 0: $\frac{n_{22}}{n_{12} + n_{22}}$ POD for event 1: $\frac{n_{11}}{n_{21} + n_{11}}$ $\in [0,1], 1 \text{ is best}$
False Alarm Rate (FAR)	The fraction of incorrect Cloud_cci reports of a	FAR for event 0:

	particular category relative to all Cloud_cci reports of this category.	$\frac{n_{21}}{n_{21} + n_{22}}$ FAR for event 1: $\frac{n_{12}}{n_{12} + n_{11}}$ $\in [0,1], 0 \text{ is best}$
Heidke Skill Score (HSS)	The HSS measures the fractional improvement of the forecast over the standard forecast.	$\frac{2 [(n_{11} n_{22}) - (n_{21} n_{12})]}{(n_{11} + n_{21}) \cdot (n_{21} + n_{22}) + (n_{11} + n_{12}) \cdot (n_{12} + n_{22})}$ $\in [-\infty, 1], 1 \text{ is best}$
Hansen-Kuiper Skill Score (HKSS)	This is a measure of correct Cloud_cci reports, with random correct and unbiased reports subtracted out.	$\frac{n_{11} n_{22} - n_{12} n_{21}}{(n_{11} + n_{21}) - (n_{12} + n_{22})}$ $\in [-1,1], 1 \text{ is best}$
Bias	Mean difference between Cloud_cci and reference data.	$\frac{n_{12} - n_{21}}{n_{11} + n_{12} + n_{21} + n_{22}}$


### 1.3.2 Datasets used for evaluation

In Table 1- Table 1-6 all reference data used in this report are listed together with the cloud and/or radiation properties considered and the type of evaluation they are used for in this report. Data of CALIPSO-CALIOP, SYNOP, BSRN, AMSR2, DARDAR and CERES are considered as validation reference with smaller errors than the difference to the Cloud\_cci product. CMSAF CLAAS-3 is considered for comparison purposes.

**Table 1-6:** Reference data used in this report including a description of the type of data, the cloud properties available and the type of reference the data is considered as (validation or comparison).

Dataset	Type of data	Variables	Type of evaluation
CALIPSO-CALIOP	Retrieval based on space-based active LIDAR measurements. (See Section A.1 for details)	Level-2 CMA, CPH and CTH	Validation
AMSR2 LWP	Space-based liquid water path over ocean based on passive microwave observations. (See Section A.2 for details)	Level-2 LWP	Validation
DARDAR	Space-based ice water path based on active LIDAR and RADAR observations. (See Section A.3 for details)	Level-2 IWP	Validation
BSRN	Ground-based observations of incoming shortwave and	Level-3C BOA SW and LW	Validation

	<p>downwelling longwave radiative fluxes. (See Section A.4 for details)</p>		
<b>SYNOP</b>	<p>Ground-based, human observations of cloud cover. (See Section A.5 for details)</p>	Level-3C CFC	Validation
<b>CERES</b>	<p>Space-based observations of shortwave and longwave radiative fluxes. (See Section A.6 for details)</p>	Level-3C TOA SW and LW	Validation
<b>CLAAS-3</b>	<p>SEVIRI-based climate data record developed and generated by EUMETSAT CM SAF for cloud product comparison. (See Section A.7 for details)</p>	Level-3C CFC all/low/mid/high, CPH, CTP, CTT, CTH, COT, CER and CWP	Comparison

	Doc: Cloud_cci+_D4.1_PVIR_v3.0.docx			
	Date: 20.11.2023			
	Issue: 3	Revision: 0	Page 12	

## 2 Evaluation of SEVIRI v3 data

This section lists the validation results for the Cloud\_cci SEVIRI Level-2 cloud and Level-3 cloud and radiation products. Cloud\_cci products are compared to reference observations that are expected to be of higher accuracy. The Section 2.1 provides pixel-based comparisons of Level-2 data to A-Train observations (CALIOP-CALIPSO, CPR-CloudSat and AMSR2). Section 2.2 contains Level-3C validation against ground-based SYNOP observations (section 2.2.1) and against CERES and BSRN in section 2.2.2. In section 0 various Cloud\_cci Level-3 variables are compared to CM SAF CLAAS-3, a SEVIRI-based Climate Data Record (CDR) generated within EUMETSAT Satellite Application Facility on Climate Monitoring ([www.cmsaf.eu](http://www.cmsaf.eu)).

### 2.1 Level-2 data

In the following two sections validation results of SEVIRI Level-2 cloud properties are presented. Cloud mask (CMA), cloud phase (CPH) and cloud top height (CTH) are validated against CALIOP pixel-based measurements in section 0. Ice water path (IWP) is validated against DARDAR (combined CloudSat radar and CALIPSO lidar product) in section 2.1.2 and Liquid water path (LWP) is validated against AMSR2 in section 2.1.3.

For matching the SEVIRI data to the reference data, SEVIRI Level-2 cloud mask, phase and height with CALIOP Cloud mask (CMA), cloud phase (CPH) and cloud top height (CTH) have been collocated with CALIOP v4 5km measurements using a common software package ([https://github.com/fouaps/atrain\\_match](https://github.com/fouaps/atrain_match)). Liquid Water Path (LWP) and Ice Water Path (IWP) have been collocated with National Snow and Ice Data Center (NSIDC) AMSR2 v1 and DARDAR v3.00 using the same software package. The validation scores presented are based on data from July 2019 for validations with CALIOP and AMSR2 and on data from February 2019 for validations against DARDAR. The latter is because of DARDAR data not being available for July 2019 yet. One should also note that the validation results against CALIOP and AMSR2 for July 2019 are very similar to February 2019, which are that's why not explicitly shown in this report.

The collocation time window between the SEVIRI and the reference data has been set to 7.5 minutes. SEVIRI pixels with high scanning angles above 70° have been removed from the collocations before validating.

#### 2.1.1 Validation of SEVIRI Level-2 CMA, CPH and CTH with CALIOP

This subsection validates SEVIRI Level-2 cloud mask (CMA), cloud phase (CPH) and cloud top height (CTH) using CALIOP LIDAR measurements as a reference.

##### Cloud mask

The cloud mask validation was separated into two scenarios: (a) counting all those CALIOP observations as clear-sky for which the reported CALIOP COT was equal to 0, and (b) additionally labelling also those CALIOP observations as clear-sky which have an CALIOP COT of greater than 0 but below 0.15. The latter scenario is included to account for and quantify the limited sensitivity of passive imagers to optically thin clouds under certain conditions.

Table 2-1 reports the cloud mask (CMA) scores and underlying number of matched CALIOP profiles. Validation against CALIOP shows a good cloud detection performance with a hitrate of 86% even with thin clouds being included. Heidke and Hansen-Kuiper skill scores are showing a good detection performance with 0.72 and 0.73, respectively. CALIOP and Cloud\_cci have a mean cloud cover of about 62% and 57%, respectively. The 5% underestimation of cloud occurrences in SEVIRI is primarily due to a lack of sensitivity of passive imager measurements to optically very thin clouds. Reclassifying optically thin clouds in the CALIOP data as clear-sky (using the CALIOP cloud optical thickness information) shows a clear improvement in the found detection scores. Scores are also comparable

for both day and night scenes (not shown). Compared to the predecessor (version 2) almost every score and statistic improved significantly due to bug fixes and optimizations.

**Table 2-1: Summary of validation scores for the cloud mask using CALIOP as reference with and without applying an optical thickness filter to CALIOP profiles.**

	Score (COT=0.0)	Score (COT=0.15)
<b>Matched profiles</b>	580 419	580 419
<b>Hirate</b>	86 %	86 %
<b>POD cloudy</b>	85 %	96 %
<b>POD clear</b>	88 %	77 %
<b>FAR cloudy</b>	8 %	22 %
<b>FAR clear</b>	21 %	4 %
<b>HSS</b>	0.72	0.72
<b>HKSS</b>	0.73	0.73
<b>Bias</b>	- 5 %	11 %

### Cloud phase

The cloud phase validation was done similarly to the cloud mask validation (previous section), thus separated into two scenarios, with, however, different definitions: (a) selecting the CALIOP cloud phase of the uppermost reported cloud layer as reference observations, and (b) selecting that CALIOP cloud phase as reference that belongs to the uppermost cloud layer after removing all top layers with an integrated COT of lower than 0.15. Also here, the latter scenario is included to account for and quantify the limited sensitivity of passive imagers to optically thin cloud layers. Further required conditions for the valid collocations is the CALIOP phase quality flag being medium (2) or high (3).

Table 2-2 reports the cloud phase (CPH) scores. Validation against CALIOP shows a good cloud phase determination performance with a hitrate of 87% even with thin clouds being included. Heidke and Hansen-Kuiper skill scores are showing a good performance with 0.74 for both, respectively. CALIOP and Cloud\_cci have a liquid cloud fraction of about 47% and 46%, respectively. Data are biased by 1% towards liquid clouds. CPH scores with the uppermost thin cloud layers removed are slightly worse compared to then including these thin cloud layers. This is likely due to the CPH neural network threshold indeed being optimized for COT=0.0.

Compared to the predecessor (version 2) almost every score and statistic improved significantly due to bug fixes and optimizations.

**Table 2-2: Summary of validation scores for the cloud phase using CALIOP as reference without applying an optical thickness filter to CALIOP profiles. Collocation time window is 7.5 minutes. The SEVIRI satellite zenith angle has been limited to 70°.**

	Score (COT=0.0)	Score (COT=0.15)
<b>Matched profiles</b>	266 948	245 096
<b>Hirate</b>	87 %	86 %
<b>POD ice</b>	87 %	93 %
<b>POD liquid</b>	87 %	81 %
<b>FAR ice</b>	11 %	21 %
<b>FAR liquid</b>	15 %	6 %
<b>KSS</b>	0.74	0.73
<b>HKSS</b>	0.74	0.74
<b>Bias</b>	-1.0 %	8.0 %

**Cloud top height**

The cloud top height (CTH) validation was done by separating the validation into three scenarios: (a) selecting the CALIOP cloud top height of the uppermost reported cloud layer as reference observations, (b) selecting that CALIOP cloud height as reference that belongs to the uppermost cloud layer after removing all top layers with an integrated COT of lower than 0.15 and (c) selecting that CALIOP cloud height as reference that belongs to the uppermost cloud layer after removing all top layers with an integrated COT of lower than 1.0. The latter scenarios are done to account for and quantify the limited sensitivity of passive imagers to optically thin cloud layers. The validation is separated into liquid and ice clouds, for which both data sources had to agree on the phase for conducting the phase stratification. For a valid pair, CALIOP phase quality has to be medium (2) or high (3) and Cloud\_cci retrieval has to have converged and cost has to be < 100.

Table 2-3 reports the CTH validation scores and number of collocation matches for all clouds, liquid clouds and ice clouds for all three scenarios. Liquid cloud biases are relatively small around zero (< 0.28 km) and are less sensitive to thin cloud layers being filtered out than ice clouds. Ranging between 1.88 km and 1.95 km, the bc-RMSE is also only weakly sensitive to COT filtering.

There is a significant underestimation of the cloud top height of ice clouds. This is mainly caused by thin high-level ice clouds which are assigned too low by the retrieval. For those clouds the signal detected by passive instruments like SEVIRI is a mixture of the cloud signal and the typically warmer atmosphere below causing a too low height assignment. Removing thin top layer clouds improves the ice cloud and total cloud agreement between CALIOP and Cloud\_cci significantly. The ice and all cloud bc-RMSE also improves with thin clouds being filtered out (6.04 km to 3.34 km for ice clouds and 4.90 km to 3.57 km for all clouds).

Figure 2-1 shows the 2-dimensional histogram of Cloud\_cci CTH (x-axis) and CALIOP CTH (y-axis). With a correlation coefficient of  $r=0.60$  the Cloud\_cci and CALIOP correlation is relatively high but the plot also shows the negative bias presented in Table 2-3 mainly due to ice phase clouds.

**Table 2-3: Summary of validation scores for the cloud top height using CALIOP as reference with and without applying optical thickness filtering to CALIOP profiles.**

	All clouds			Liquid clouds			Ice clouds		
	COT=0.0	COT=0.15	COT=1.0	COT=0.0	COT=0.15	COT=1.0	COT=0.0	COT=0.15	COT=1.0
<b>Matches</b>	258557	237755	200201	105870	110802	105840	119413	110802	52529
<b>Bias [km]</b>	-2.51	-1.33	-0.17	-0.12	-0.09	0.28	-4.07	-3.01	-1.89
<b>bc-RMSE [km]</b>	4.90	4.25	3.57	1.88	1.95	1.94	6.04	5.03	3.34

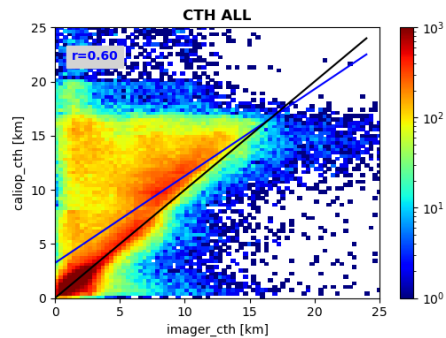


Figure 2-1 Two-dimensional histogram of Cloud\_cci CTH (x-axis) and CALIOP CTH (y-axis). Black line is the 1:1 line and blue line indicates the linear regression line.

### 2.1.2 Validation of SEVIRI Level-2 IWP with DARDAR

Reference for the IWP validation is the DARDAR-cloud product in version 3.00. DARDAR-cloud contains the Ice Water Content (IWC) in kg/m<sup>3</sup> of each of its vertical layers. To convert it to a comparable IWP, IWC was multiplied by the layer thickness (60m) and vertically integrated afterwards. Collocations are limited to daytime by solar zenith angle (< 75°) and to a satellite zenith angle of 70°. To account for the DARDAR footprint size, the up to 3 closest Cloud\_cci IWP observations that fall into that footprint had to be averaged. The radius of influence for nearest neighbour search was set to 1.5 km. Collocations where Cloud\_cci reported an ice fraction of less than 90% were excluded from the validation. DARDAR profiles where any layer is reported to be

- Presence of liquid unknown (DARMASK\_Simplified\_Categorization: -2)
- Supercooled water (DARMASK\_Simplified\_Categorization: 3)
- Stratospheric clouds (DARMASK\_Simplified\_Categorization: 8)
- Liquid cloud (DARMASK\_Simplified\_Categorization: 11)
- Warm rain + liquid clouds (DARMASK\_Simplified\_Categorization: 12)
- Cold rain+ liquid clouds (DARMASK\_Simplified\_Categorization: 13)
- Rain may be mixed with liquid (DARMASK\_Simplified\_Categorization: 14)
- Multiple scattering due to supercooled water (DARMASK\_Simplified\_Categorization: 15)

were removed from the validation to only have homogeneous ice clouds. Footprint-averaged Cloud\_cci IWP is restricted to an IWP between 0 and 2000 g/m<sup>2</sup> to remove outliers, which in particular exist in Cloud\_cci data with quite some data points exceeding 2000 g/m<sup>2</sup>. Applying this threshold removes 0.53% of all collocation pairs and improves the correlation as well as the bias significantly. Cloud\_cci IWPs within the DARDAR footprint which are flagged as a bad retrieval (retrieval did not converge or retrieval cost > 100.0) were also masked.

Generally it should be noted that the calculated statistics are highly sensitive to small changes in the data masking and preparation and should therefore only be carefully compared to other sources.

Figure 2-2 shows the IWP validation statistics, data distribution and the sample size. With a correlation coefficient of 0.55, Cloud\_cci and DARDAR are in relatively good agreement. There is a general overestimation of Cloud\_cci IWP with a bias of about 22 g/m<sup>2</sup>. Whereas DARDAR IWP highest values reach up to about 1000 g/m<sup>2</sup> Cloud\_cci has much higher values (also visible in the distributions). The discrete Cloud\_cci values distribution at lower IWPs (< 10 g/m<sup>2</sup>), visible in the bottom-left plot of Figure 2-2, are due to Cloud\_cci IWP data being store at a resolution of 1 g/m<sup>2</sup>. For IWP values between 10 and 30 g/m<sup>2</sup> the agreement looks reasonable. For values above 30 g/m<sup>2</sup> (according to DARDAR), however, a strong positive bias in Cloud\_cci data is found, with Cloud\_cci values partly being one order of magnitude higher than DARDAR. The reason for this is still unclear.

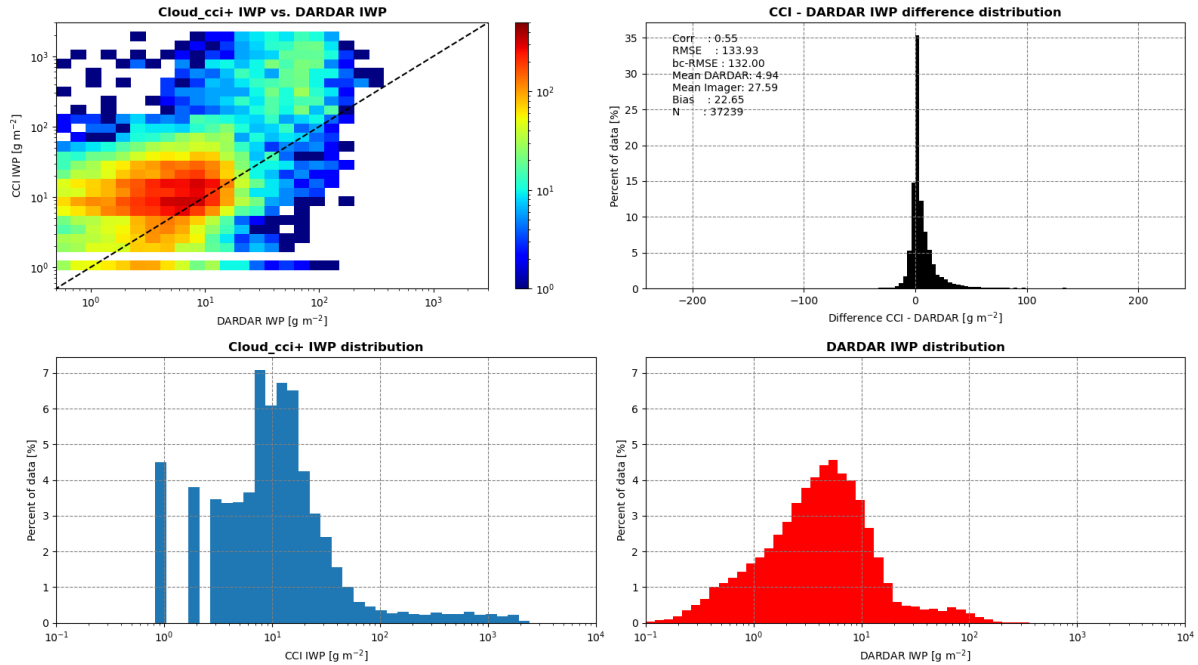


**Figure 2-2** Validation results for Cloud\_cci with respect to DARDAR Ice Water Path (IWP). Upper left panel shows the 2-dimensional histogram of DARDAR IWP (x-axis) vs. Cloud\_cci IWP (y-axis) using a log-log scale. Bin size is  $10 \times 10 \text{ g m}^{-2}$ . Black dashed line is the 1:1 line. Upper right panel shows the CCI - DARDAR IWP difference distribution as % of the whole number of collocated data pair as well as the corresponding statistics. Lower left and right histograms show the Cloud\_cci and DARDAR IWP distribution, respectively using a log scale on the x-axis. Statistics are shown in the upper right image.

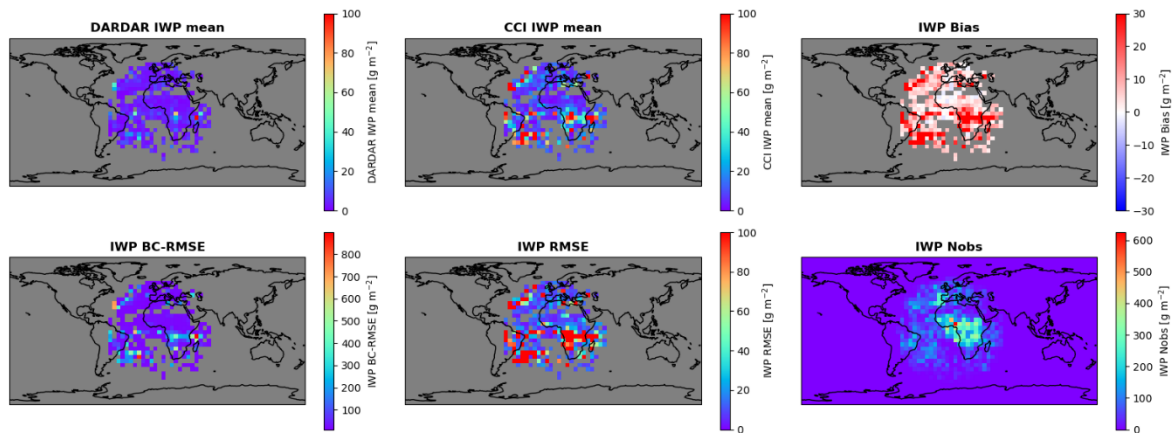


**Figure 2-3** Spatial distribution of IWP validation statistics (DARDAR mean, Cloud\_cci mean, bias, bc-RMSE, RMSE, number of observations) in  $5^\circ \times 5^\circ$  boxes. No statistics were calculated for boxes with less than 30 observations



### 2.1.3 Validation of SEVIRI Level-2 LWP with AMSR2

Reference for the LWP validation are the AMSR2 products. Due to the large AMSR2 footprint, up to 8 closest Cloud\_cci LWP observations that fall into that footprint had to be averaged including clear-sky pixels counting with a LWP of 0. The radius of influence for nearest neighbour search was set to 5.4 km. Please note that a circle for the nearest neighbour radius is only an approximation for the elliptical AMSR2 footprint. AMSR2 footprints for which Cloud\_cci reported an ice fraction of greater-equal 10% were excluded from the validation. This is done to excluded cases (ice clouds) for which the microwave signal is impacted by significant scattering at ice particles, which are unfavourable circumstances for the retrieval of liquid water path from AMSR2. As AMSR2 observations are reliable over ocean only, all land regions were also excluded from this LWP validation. Collocations are limited to daytime by solar zenith angle ( $< 75^\circ$ ). For a valid collocation pair at least 50% of the possible 8 neighbours within each footprint have to be found valid. If at least one neighbour in the footprint is flagged with a bad retrieval (retrieval did not converge or retrieval cost  $> 100.0$ ) the footprint is excluded. To avoid AMSR2 LWP being contaminated by rain, validation is restricted to an LWP between 0 and 170  $\text{g/m}^2$ . Cloud\_cci LWP is restricted to an LWP between 0 and 500  $\text{g/m}^2$ . To ensure AMSR2 data quality, only collocations with “QualityFlag=0” and “PixelStatus=0” were used.

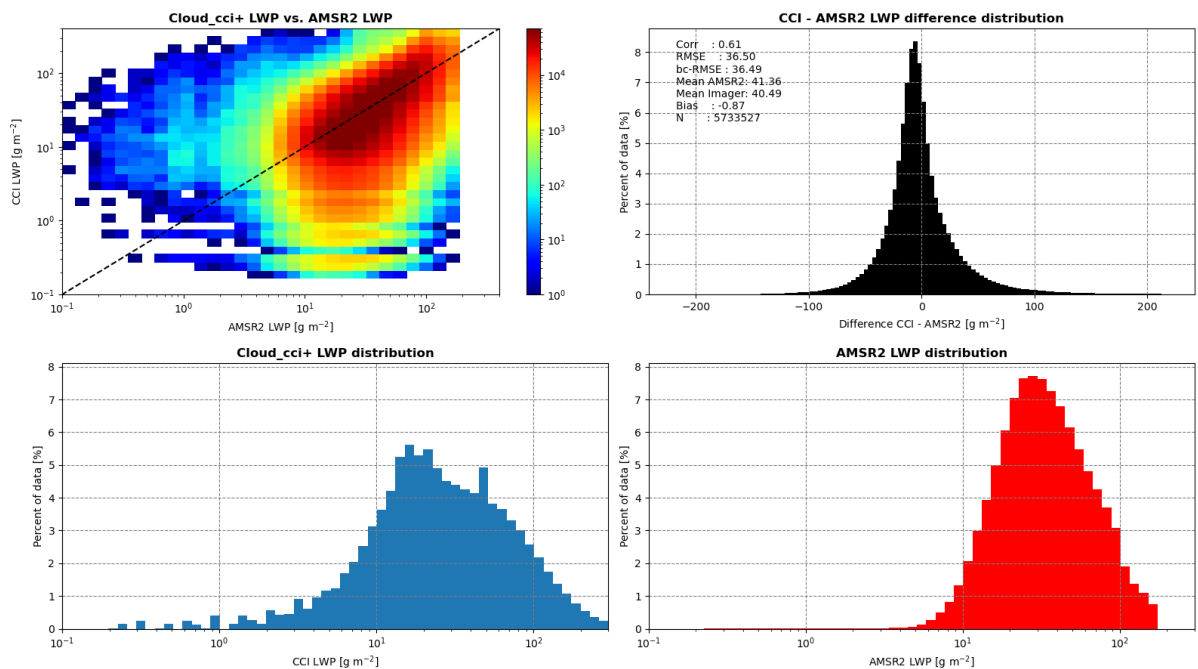


Figure 2-4 reports the LWP validation statistics, number of data pairs and data distribution. The validation reveals that Cloud\_cci is in good agreement with AMSR2 LWP and underestimates it only by about  $-0.87 \text{ g/m}^2$ . Cloud\_cci and AMSR2 LWP are correlated with a Pearson correlation

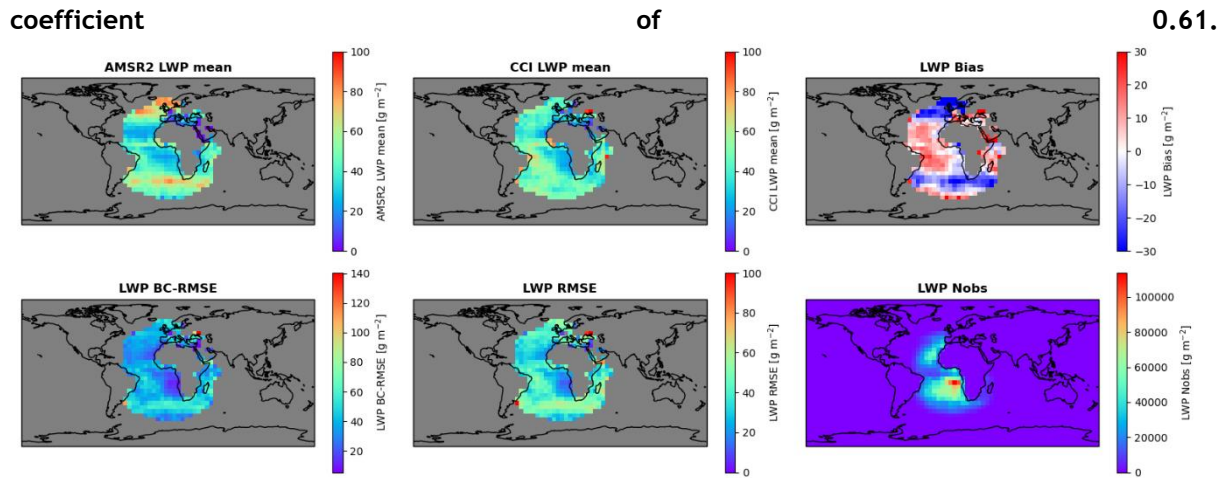


Figure 2-5 shows the spatial distribution of statistics in 5° x 5° box and indicates the coverage area. The main contribution to a negative bias is from the areas in the southern and northern Atlantic which are nearly compensated by the middle Atlantic Ocean. Also bc-RMSE and RMSE are highest in the southern Atlantic region.

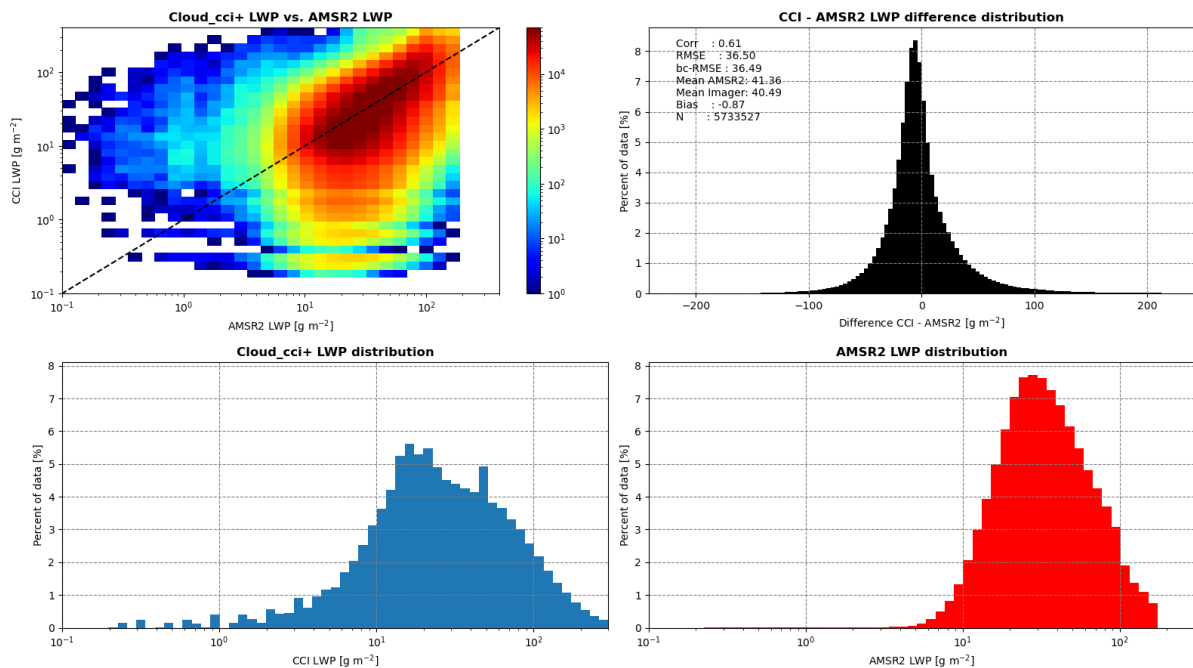
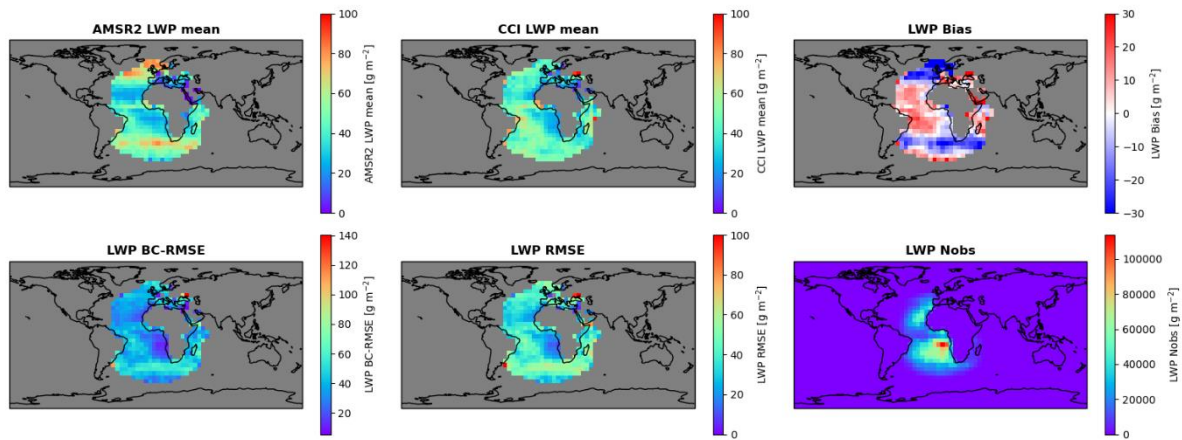


Figure 2-4 Validation results of Cloud\_cci and AMSR2 liquid water path (LWP). Upper left panel shows the 2-dimensional histogram of AMSR2 LWP (x-axis) vs. Cloud\_cci LWP (y-axis) using a log-log scale. Bin size is 5x5 g m<sup>-2</sup>. Black dashed line is the 1:1 line. Upper right panel shows the CCI - AMSR2 LWP difference distribution as % of the whole number of collocated data pair as well as the corresponding statistics. Lower left and right histograms show the Cloud\_cci and AMSR2 LWP distribution, respectively using a log scale on the x-axis. Statistics are shown in the upper right image.



**Figure 2-5** Spatial distribution of LWP validation statistics (AMSR2 mean, Cloud\_cci mean, bias, bc-RMSE, RMSE, number of observations) in 5° x 5° boxes.

## 2.2 Level-3 data

### 2.2.1 Validation of SEVIRI Level-3C CFC with SYNOP data

Human SYNOP observations of cloud fraction have been collected, quality-controlled and aggregated to monthly means for all SYNOP sites within the SEVIRI disk. Figure 2-6 and Figure 2-7 show the statistics for February and July 2019. The CFC biases are between 10 and 13%, thus there is a slight overestimation of CFC by Cloud\_cci, which seems primarily be introduced by regions with large SEVIRI viewing angles, e.g. Middle East and South America. Another feature is the strong underestimation of cloud fraction in South West Africa in February, which needs further investigation.

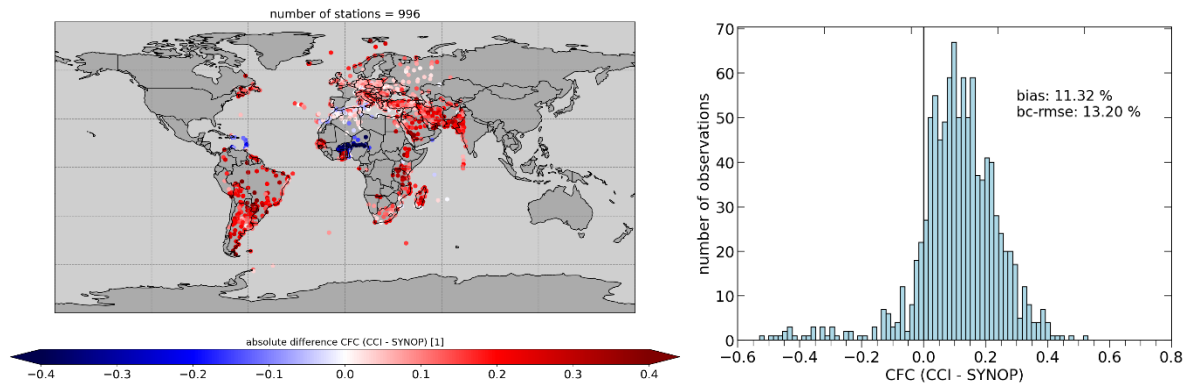


Figure 2-6 Left: Bias of Cloud\_cci SEVIRI v3 L3C cloud fraction (CFC) against human SYNOP observation for February 2019. Right: Histogram of L3C differences.

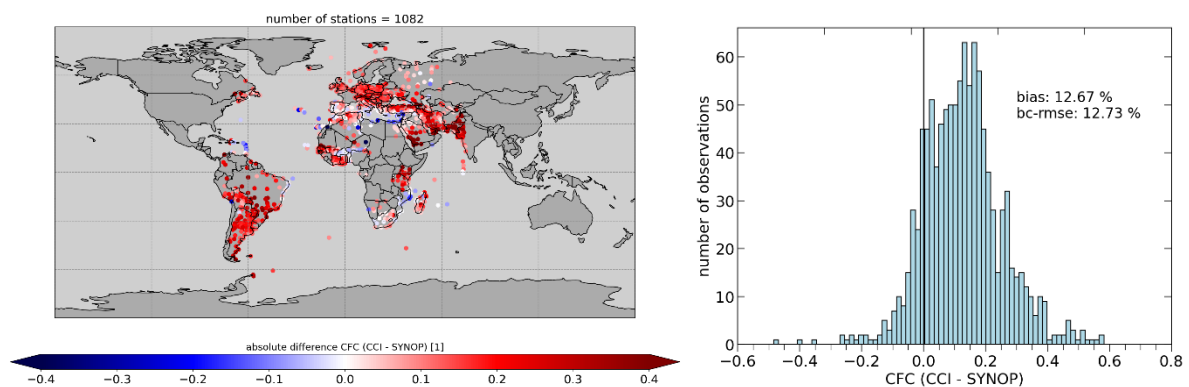


Figure 2-7 As Figure 2-6 but for July 2019.

### 2.2.2 Validation of SEVIRI Level-3 radiative fluxes with CERES and BSRN

Space-based CERES observations of top of atmosphere radiation as well as ground measurements of downwelling SW and LW radiation taken at sites of the international Baseline Surface Radiation Network (BSRN) were used to validate Cloud\_cci TOA and BOA radiative fluxes.

### CERES

Figure 2-8 shows mean maps for top-of-atmosphere (TOA) shortwave radiative fluxes from Cloud\_cci SEVIRI v3, CERES and the differences for July 2019 for both allsky and clear-sky conditions. For allsky fluxes, regional patterns are very similar between SEVIRI and CERES with high values in desert regions (e.g Sahara, Middle East) and oceanic regions with high cloud fraction, e.g. Stratocumulus in the South East Atlantic, in the Tropics and North-Hemispheric Storm tracks. Low values are found in both products for trade cumulus regions in the western part of the sub-tropical Atlantic. Largest negative biases are found for Northern hemispheric storm track region (underestimation by SEVIRI), while largest positive biases (overestimation by SEVIRI) are found in the desert regions of the Northern Hemisphere. These biases are already visible in the clear-sky fluxes which suggested that these are rather caused by surface properties in the broadband flux modelling instead of in the derived cloud properties. For long-wave fluxes (Figure 2-9), the agreement in regional patterns between SEVIRI and CERES seems even better (than for shortwave fluxes) with biases being more uniform, negative biases nearly everywhere which are of smaller amplitude.

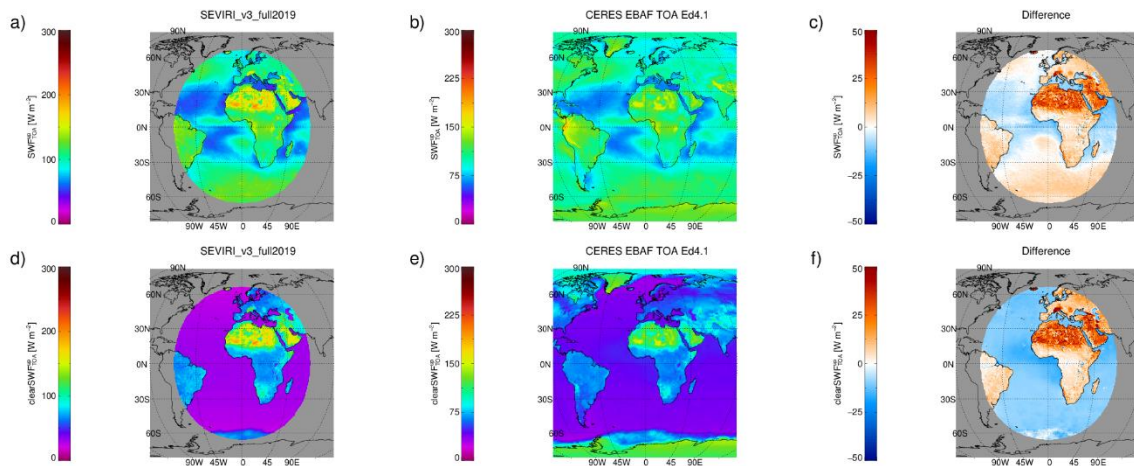


**Figure 2-8** Top row: Mean maps of TOA upwelling all-sky shortwave (WV) radiative flux for 2019 for Cloud\_cci SEVIRI v3 (left), CERES (middle) and the difference (right). Bottom row: same maps but for clear-sky.

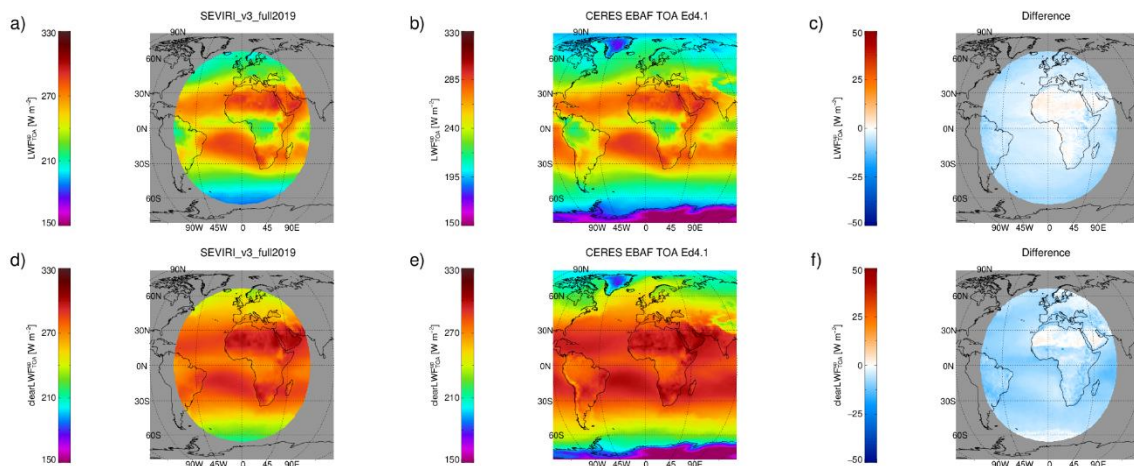


**Figure 2-9** Same as Figure 2-8 but for longwave fluxes.

Figure 2-10 reports two-dimensional frequency distributions and validation scores for monthly mean TOA upwelling (allsky) shortwave fluxes for Cloud\_cci SEVIRI v3. The histograms reveal an excellent agreement of all Cloud\_cci dataset with CERES with standard deviations ranging from 2.9 W/m<sup>2</sup> (longwave) to 12.3 W/m<sup>2</sup> (shortwave). Biases are all slightly negative ranging from -4.85 (longwave) to -3.6W/m<sup>2</sup> (shortwave). Please note that the deviations to CERES in bias map in Figure 2-8 are shown exaggerated (objectively speaking) by the selected colour bar scale. These deviation are indeed include in Figure 2-10 but less obvious because (a) they spread over a certain range of absolute values and (b) of the selected range of the axes in this Figure. The maps for February 2019 are comparable to July and thus not further shown and discussed here. In Table 2-4 the validation scores (including February and July 2019) are additionally stratified by USGS surface type. Biases in shortwave fluxes are largest for areas with higher albedo surfaces, e.g. Open Shrublands, Snow/ice and Barren/Sparsly\_Vegetated areas. Only (slight) negative bias is found for lakes/oceans, which is important as approx. half of SEVIRI field of view is ocean. Largest standard deviations are for example found for Snow/Ice surfaces and Evergreen Needle leaf Forests. For longwave fluxes, the biases are generally negative for all surface types, most prominent for Snow/Ice surfaces. Standard deviations are smaller compared to shortwave fluxes and range from 1.2 W/m<sup>2</sup> 3.7 W/m<sup>2</sup>.

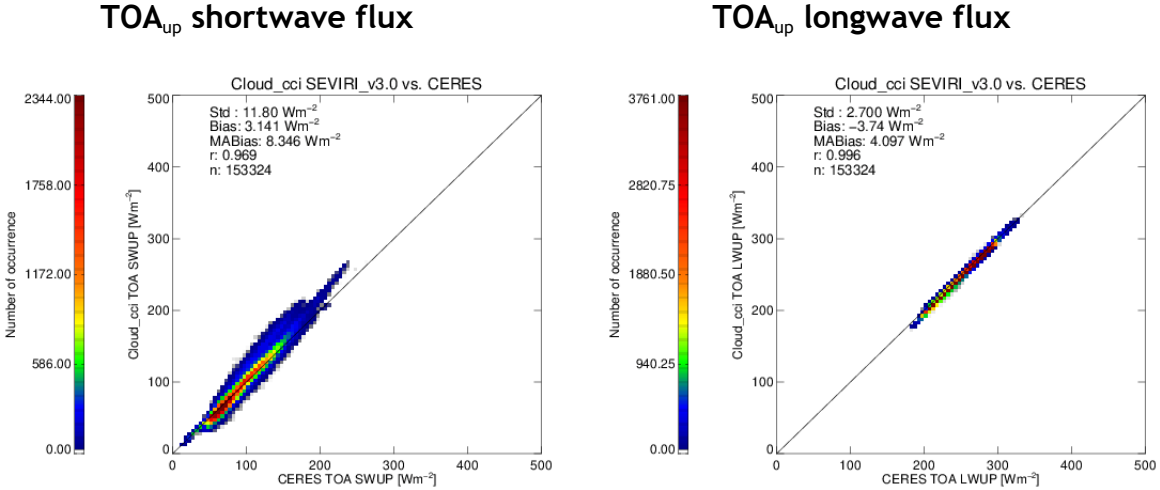


**Figure 2-10** Cloud\_cci SEVIRI top of atmosphere (TOA) monthly mean upwelling shortwave (left) and longwave flux (right) validation against to CERES EBAF-TOA Ed4.0. Data basis contains monthly mean data including all months of 2019.

**Table 2-4** *Cloud\_cci SEVIRI top of atmosphere (TOA) monthly mean upwelling shortwave flux validation against to CERES EBAF-TOA Ed4.0 stratified by USGS surface type. Data basis contains monthly mean data including all months in 2019.*

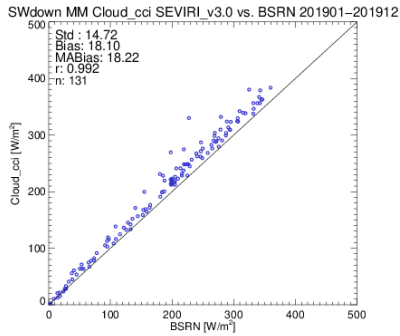
USGS class	TOA <sub>up</sub> shortwave flux		TOA <sub>up</sub> longwave flux	
	Bias [Wm <sup>-2</sup> ]	Std [Wm <sup>-2</sup> ]	Bias [Wm <sup>-2</sup> ]	Std [Wm <sup>-2</sup> ]
Water	-1.46115	8.02624	-4.37320	1.99943
Evergreen Needle leaf Forest	8.75344	16.7210	-4.74912	1.77747
Evergreen Broadleaf Forest	4.33362	6.66073	-4.72927	3.45157
	-	-	-	-
Deciduous Broadleaf Forest	7.87460	10.9251	-5.79120	2.55947
Mixed Forests	9.52639	15.7018	-4.39419	2.04528
Closed Shrublands	0.296728	4.78556	-3.12119	1.57716
Open Shrublands	11.2635	11.4086	-2.59408	2.91306
Woody Savannas	4.94857	6.12785	-2.73035	2.88419
Savannas	5.46440	5.99804	-3.31408	2.84981
Grasslands	12.0190	13.8883	-3.51204	3.44127
Permanent Wetland	4.24713	7.20981	-3.70011	3.54162
Croplands	7.62649	11.7304	-3.37627	2.50384
Urban and Built-Up	6.17238	9.40416	-4.35675	1.91198
Cropland/Natural Vegetation Mosaic	6.74563	10.1142	-2.83248	3.56370
Snow and Ice	25.8641	27.7880	-8.78115	3.01184
Barren or Sparsely Vegetated	24.5775	10.8301	-0.106548	2.70988

## **BSRN**

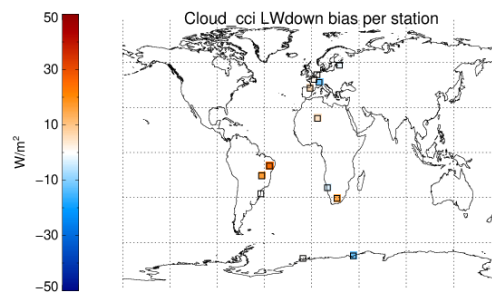
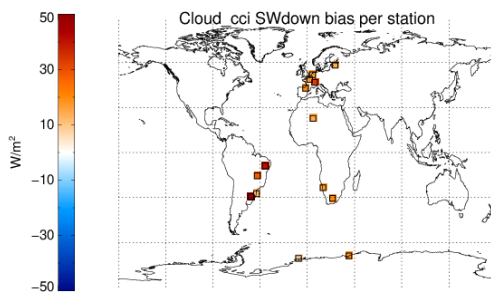
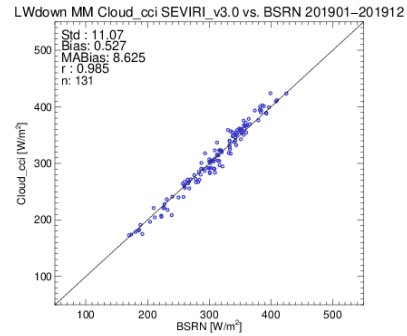
BSRN stations measure direct, diffuse and global downwelling shortwave and longwave fluxes in 1 min temporal resolution. The manned stations are located at positions, which are representative of a relatively large surrounding area for the use in satellite data validation among others. The 1-min data was aggregated to monthly averages which were used as validation data.

Figure 2-11 shows scatter plots and validation scores for monthly mean BOA downwelling shortwave and longwave radiation for Cloud\_cci SEVIRI v3 including February and July 2019. Confirming the good TOA validation results reported in previous subsection, also the BOA validation against BSRN highlights the good quality of the SEVIRI radiative flux products. Standard deviations are 13.9 W/m<sup>2</sup> for shortwave and 19.1 W/m<sup>2</sup> for longwave. The bias for longwave is smaller (5.6 W/m<sup>2</sup>) than for shortwave (17.5 W/m<sup>2</sup>). Correlations are very high (above 0.96). The shown bias maps indicate that there is at least one shortwave station (in Brazil) and one longwave stations (in the Alps) for which the biases seem amplified, which needs further investigation.

### BOA<sub>down</sub> shortwave flux



### BOA<sub>down</sub> longwave flux



**Figure 2-11** Cloud\_cci SEVIRI bottom of atmosphere (BOA) monthly mean downwelling shortwave flux validation (left) and downwelling longwave flux (right) against to BSRN. Data basis contains monthly mean data for all months in 2019.



### 2.2.3 Intercomparison against CM-SAF CLAAS-3

In this section the Cloud\_cci SEVIRI v3 products are compared to another, well-established, satellite-based dataset called “Cloud property dAtaset using SEVIRI” (CLAAS) produced by the EUMETSAT Satellite Application Facility on Climate Monitoring (CM-SAF). We compared Cloud\_cci+ July 2019 data to its latest version 3 (CLAAS-3; [https://doi.org/10.5676/EUM\\_SAF\\_CM/CLAAS/V003](https://doi.org/10.5676/EUM_SAF_CM/CLAAS/V003)). CLAAS-3 is like Cloud\_cci+ based on geostationary SEVIRI sensor measurements onboard Meteosat Second Generation (MSG) satellites. The basis for all comparisons are monthly averages on a regular lat/lon grid (Level-3C in ESA Cloud\_cci notation). CLAAS-3 monthly averages come on a 0.05° grid and thus had to be resampled to the 0.5° Cloud\_cci Level-3C grid using bucket resampling.

Table 2-5 presents disk mean values for Cloud\_cci and CLAAS-3 and the bias between the both datasets (Cloud\_cci - CLAAS-3) over all grid cells for which both datasets have data.

**Table 2-5** *Cloud\_cci and CLAAS-3 disk mean values and the biases between the two datasets (CCI - CLAAS-3) for the compared variables.*

Variable	Unit	Mean Cloud_cci+	Mean CLAAS-3	Bias
CFC	%	66.3	65.4	0.9
CFC_low	%	28.9	25.5	3.4
CFC_mid	%	15.8	14.3	1.6
CFC_high	%	18.9	24.9	-6.0
Liquid Cloud Fraction	%	55.0	66.6	-11.2
CTP	hPa	615.2	557.4	57.9
CTT	K	261.4	253.9	7.5
CTH	km	4.9	5.6	-0.7
COT	1	7.3	10.7	-3.5
CER	µm	15.2	19.9	-5.0
IWP	g m <sup>-2</sup>	96.2	149.2	-63.5
LWP	g m <sup>-2</sup>	60.2	121.4	-64.0

#### Cloud fraction

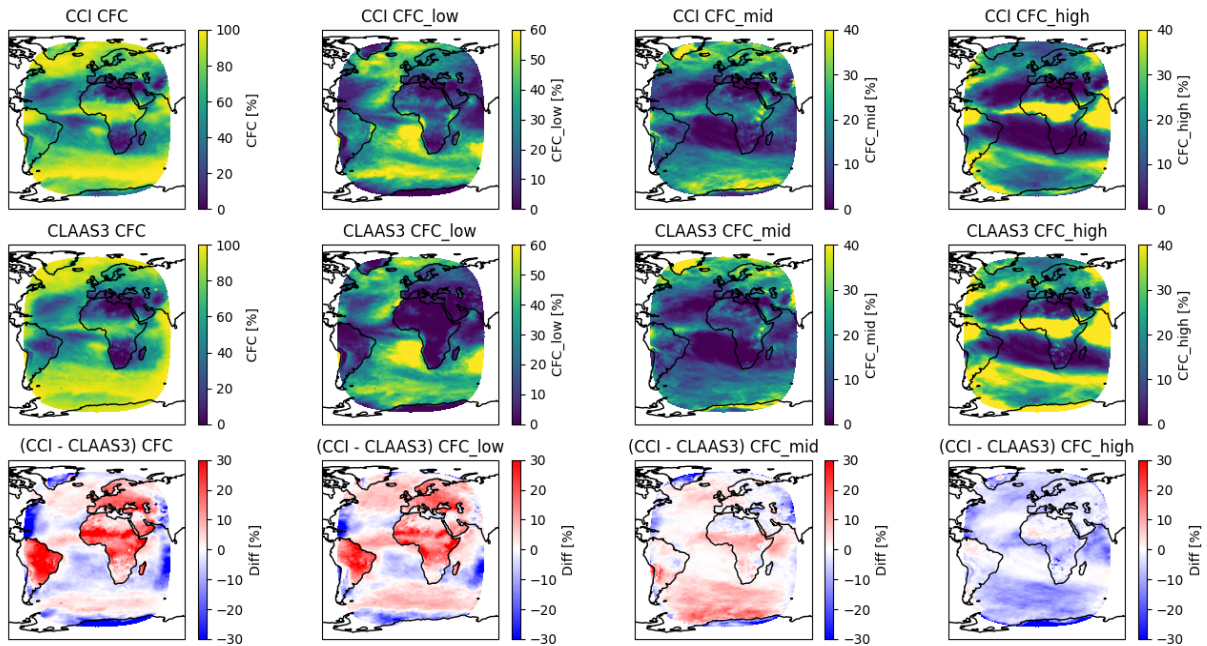


Figure 2-12 shows the comparison of monthly mean cloud fraction (CFC). The first row contains Cloud\_cci+ products, the second row the CLAAS-3 products and the third row the difference between the datasets. Compared is CFC and CFC of low-, mid- and high-level clouds following the cloud top pressure classification in [Rossow and Schiffer \(1999\)](#). Discussed biases are taken from Table 2-5.

CFC is typically higher in CLAAS-3 over the ocean and lower over land compared to Cloud\_cci. Especially at the edge of the disk over ocean CLAAS-3 CFC seems artificially too high. On disk average, CLAAS-3 is about 0.9% lower than Cloud\_cci. Cloud\_cci has about 3.4% (1.6%) more low-level (mid-level) clouds but over 6% less high-level clouds. The underestimation in high-level and overestimation of mid- and low-level cloud amount could be explained with a typically lower cloud top height in Cloud\_cci so that more clouds are assigned to the lower levels and thus missing in the highest level. On disk average low-, mid- and high-level cloud differences balance out so that the bias is close to 0 (< 1%) supporting the possible explanation above.

Overall the CFC patterns look quite comparable and disk-mean biases are quite low but locally large differences can be found. Reasons for that are first the fundamentally different approaches of detecting clouds as well as the different retrieval schemes necessary for the height assignment.

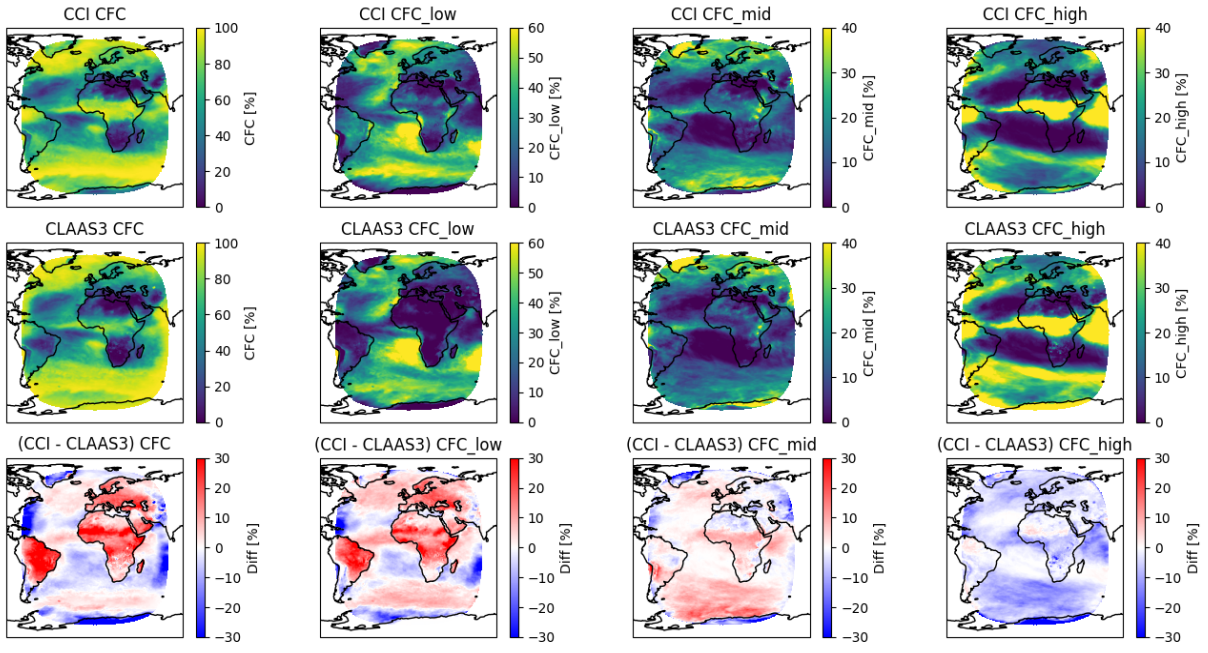


Figure 2-12 Intercomparison of ESA Cloud\_cci cloud fractional cover (CFC) with CM-SAF CLAAS-3. The first row contains Cloud\_cci+ products, the second row the CLAAS-3 products and the third row the difference between the datasets. Values are in %.

**Cloud microphysics**

Comparisons of Cloud Optical Thickness (COT), Cloud Effective Radius (CER), Cloud Water Path (CWP), Liquid Cloud Fraction (LCF) are shown in

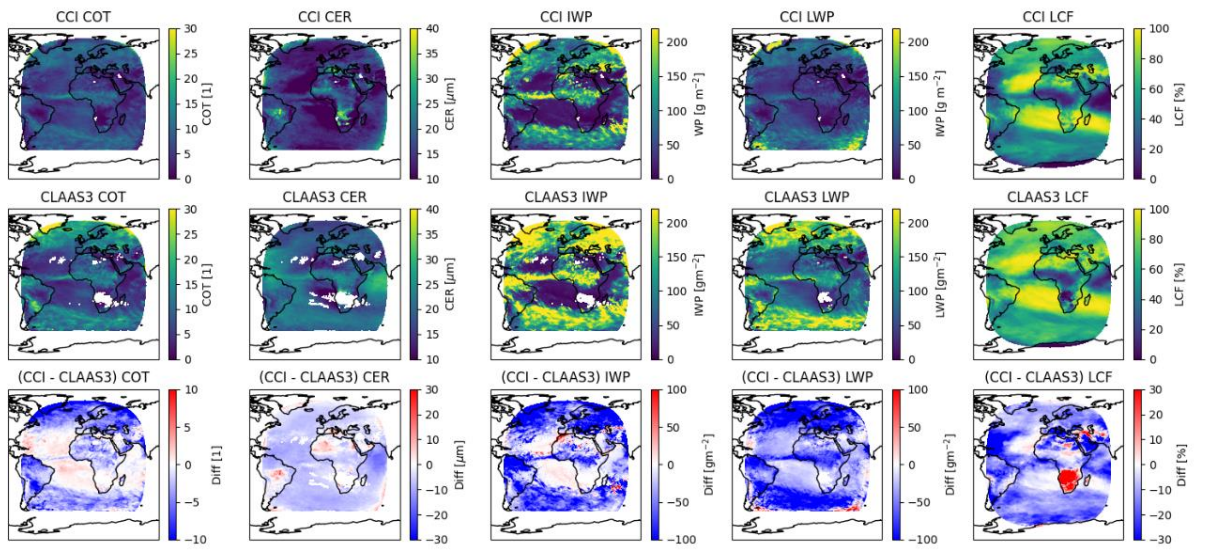



Figure 2-13. Different column align with different variables. Top row contains Cloud\_cci products, middle row presents the CLAAS-3 products and bottom row shows the difference between both. The COT, CER, IWP and LWP data cut-off at the southern end of the disk is because those variables are only retrieved during daytime conditions. Missing values within the CLAAS-3 disk is due to a minimum

	Doc: Cloud_cci+_D4.1_PVIR_v3.0.docx			
	Date: 20.11.2023			
	Issue: 3	Revision: 0	Page 28	

number of cloudy level-2 observations required for a valid level-3 pixel in the code. Bias in the following discussion are taken from Table 2-5.

Over areas where ice clouds are dominating, CLAAS-3 COT is higher than Cloud\_cci. However, liquid-dominated areas are showing a positive bias, i.e. Cloud\_cci COT has higher optical thicknesses. This is likely because the Cloud\_cci retrieval algorithm is having more problems with retrieval of thin ice clouds, as already discussed in the CTH validation (section 2.1.1). However on disk average positive and negative deviations compensate so that the bias indicates CLAAS-3 to be higher by about 3.5. The CER of Cloud\_cci and CLAAS-3 is quite comparable but on disk average Cloud\_cci CER is about 5  $\mu\text{m}$  lower. Spatial CER patterns are similar.

Cloud\_cci IWP and LWP are derived from COT and CER, as in CLAAS, thus features their patterns. Over most of the disk, IWP is substantially higher in CLAAS-3, consistently with the disk mean bias of about  $-63 \text{ g m}^{-2}$ . Concerning LWP, CLAAS-3 has a about 64  $\text{g m}^{-2}$  higher LWP mean, most dominant in the regions with frequent cloud occurrences.

Over most of the disk, the frequency of liquid clouds in Cloud\_cci is lower than in CLAAS-3. In regions with commonly low-lying liquid stratus the deviations are smallest. The LCF over the southern African continent differ severely between both products. This could likely be explained by the low cloud amount (limited number of observations) in this also high elevated area making the means not really representative. On global average we find Cloud\_cci LCF to be about 11% lower than in CLAAS-3.

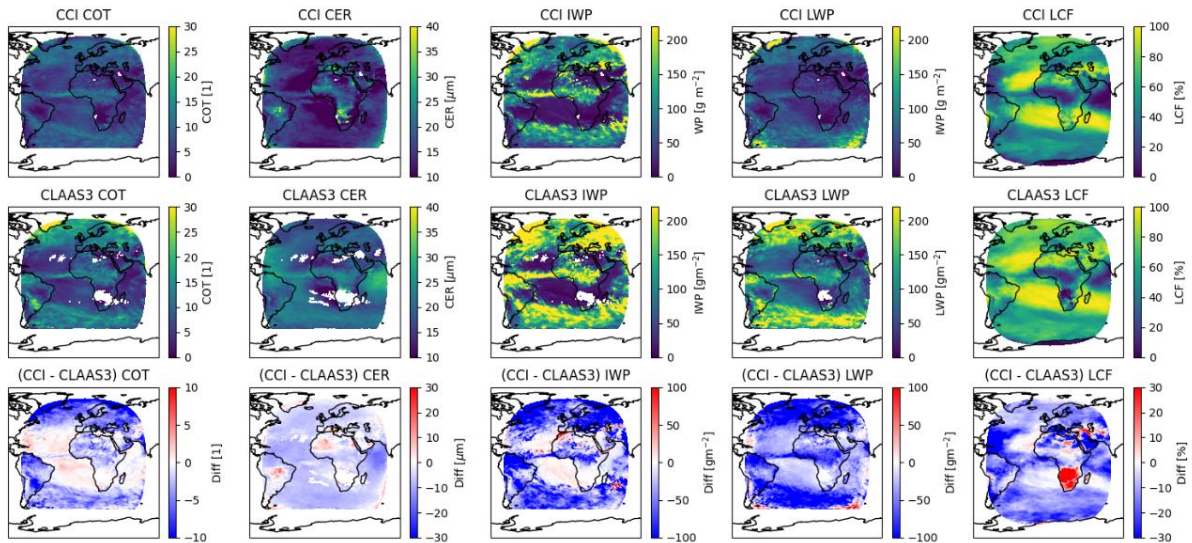


**Figure 2-13** Intercomparison of ESA Cloud\_cci cloud microphysics products with CM-SAF CLAAS-3: Cloud Optical Thickness (COT), Cloud Effective Radius (CER), Cloud Water Path (CWP), Liquid Cloud Fraction (LCF). Top row: Cloud\_cci products, middle row: CLAAS-3 products and bottom row: the difference between both.

### Cloud top products

The retrieved Cloud\_cci mean Cloud Top Pressure (CTP) as shown in

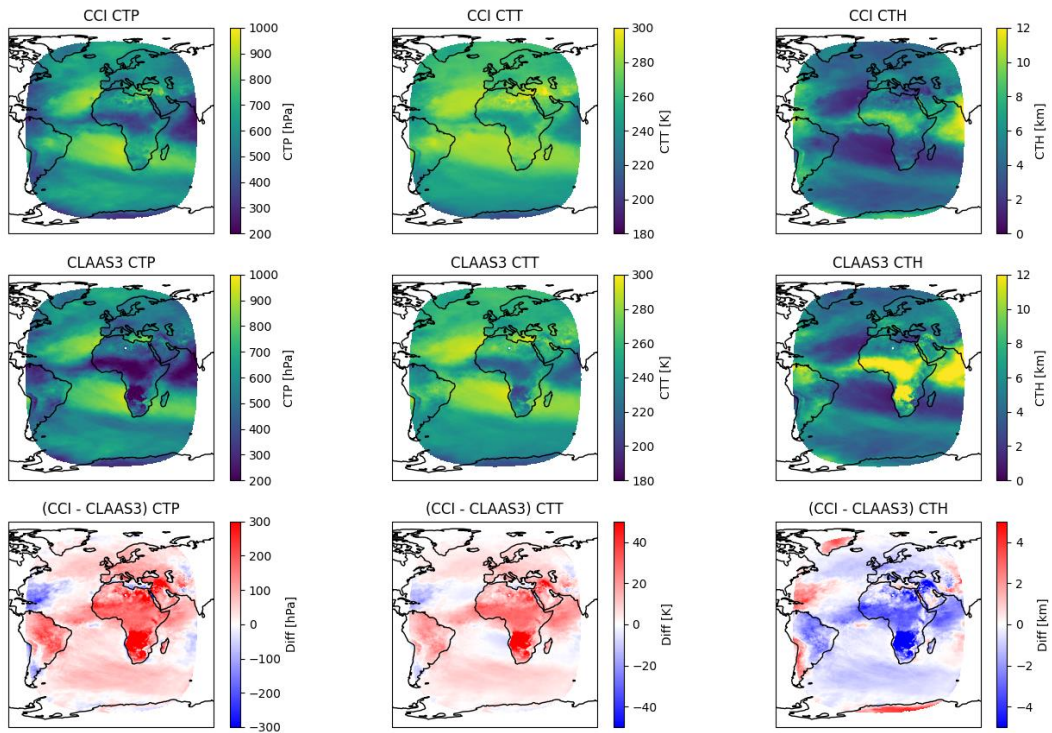
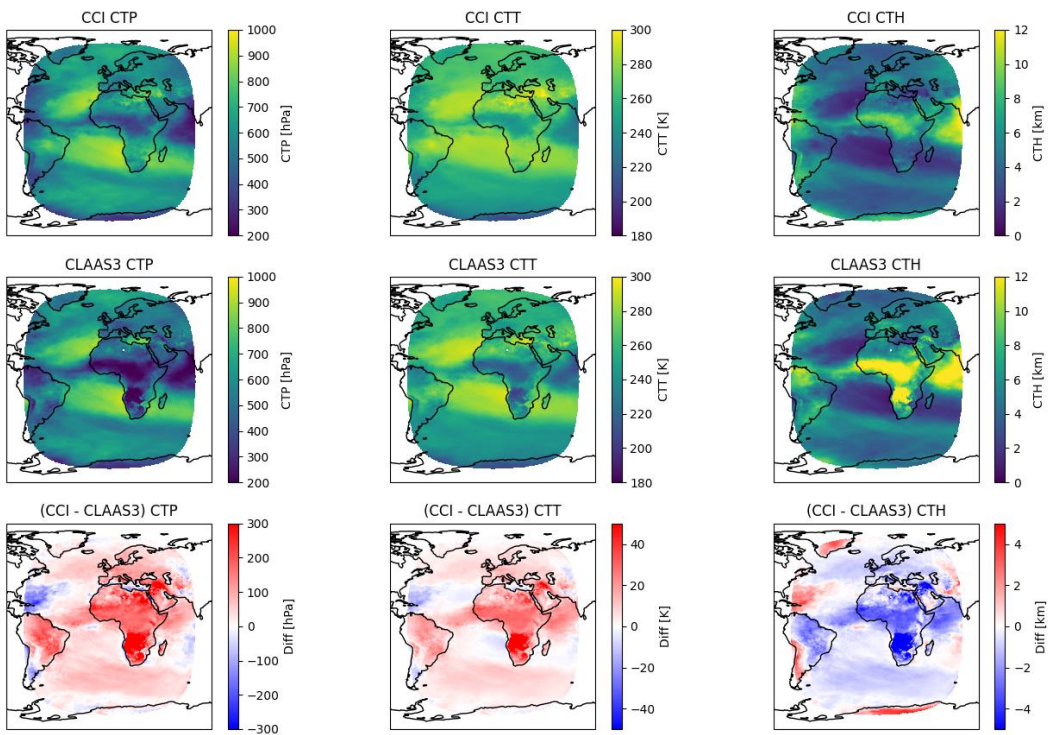
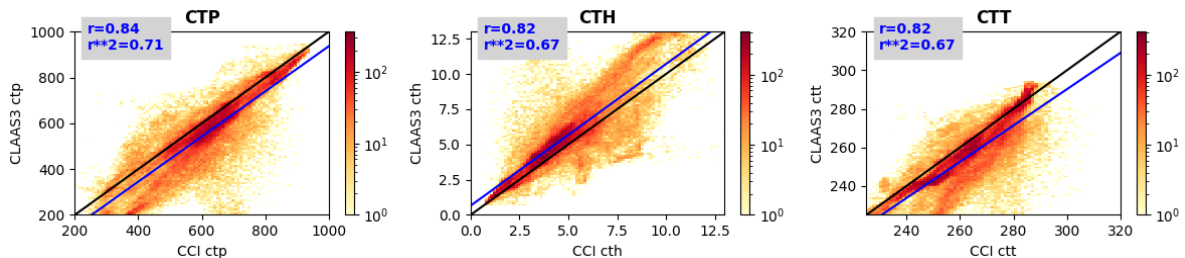


Figure 2-14 is higher than CLAAS over almost the whole disk indicating overall lower retrieved cloud tops in Cloud\_cci compared to CLAAS-3. This is consistent with the CTH validation in section 2.1.1. Cloud Top Temperature (CTT) and Cloud Top Height (CTH) are derived from CTP using vertical profiles from the ERA5 reanalysis, thus feature the same characteristics as CTP (CTH inverted). CTT is also higher than CLAAS-3 over the whole disk and CTH is lower over the whole disk. As for the cloud microphysics variables above the South African continent shows highest deviations due to the low cloud amount limiting the number of observations used for mean calculation for these pixels as well as the high elevation making retrieval more difficult. The mean biases for CTP, CTT and CTH are approximately 58 hPa, 8 K and -700 m, respectively. Negative biases indicate CLAAS-3 being higher than Cloud\_cci.



**Figure 2-14** Intercomparison of ESA Cloud\_cci cloud top products with CM-SAF CLAAS-3: Cloud Top Temperature (CTT), Cloud Top Height (CTH), Cloud Top Pressure (CTP). Top row: Cloud\_cci+ products, middle row: CLAAS-3 products and third row: difference between the datasets.

The scatter plots in Figure 2-15 show the relation of Cloud\_cci and CLAAS-3 cloud top parameters. The black solid line is the 1:1 line and the blue solid line is the linear regression. The scatter plots also show the underestimation of Cloud\_cci cloud tops even though the correlation coefficient of the cloud top variables are relatively high above 0.8. Overall the CTP correlation is highest with 0.84, followed by CTH and CTT with 0.82.



**Figure 2-15** Two-dimensional histograms of Cloud\_cci (x-axis) and CLAAS-3 (y-axis) CTP, CTH, CTT. Black line indicates the 1:1 line. Blue line is the linear regression line. The grey box contains the Pearson correlation coefficient (r) and its square (r\*\*2) of the two variables.

### 3 Evaluation of SLSTR v3 data

#### 3.1 Level-2 data

##### 3.1.1 Validation of SLSTR Level-2 LWP with AMSR2

In this section AMSR2 Unified L2B Global Swath Surface Precipitation dataset (Kummerow et. all. 2020) version 1, is used as reference for the LWP product. There is no pixel-based uncertainty reported for AMSR2 LWP. Coincidences criteria considered are 15 minutes difference between the two measurements and 5 km distance between the centre of AMSR2 footprint and Cloud\_cci pixels. All Cloud\_cci LWP observations that fall into that distance has been averaged including clear-sky pixels counting with a LWP of 0. AMSR2 footprints that include Cloud\_cci retrieval that don't pass the quality control were excluded from the validation.

As AMSR2 observations are reliable over ocean only, consequently all land regions were also excluded from this LWP validation. Only AMSR2 data that has the highest confidence of the best retrieval are considered in this validation. In particular we required these AMSR2 flags: pixel status = 0, quality flag = 0, surface type = 1.

Results for July 2019 are presented in **Fehler! Verweisquelle konnte nicht gefunden werden.** and show a correlation coefficient of 0.62 with a bias of 49 g/m<sup>2</sup>. Note that due to the time coincidence criteria, only points between 60°N and 80°N are included into this analysis, (SLSTR is in a morning orbit and AMSR2 in an afternoon orbit).

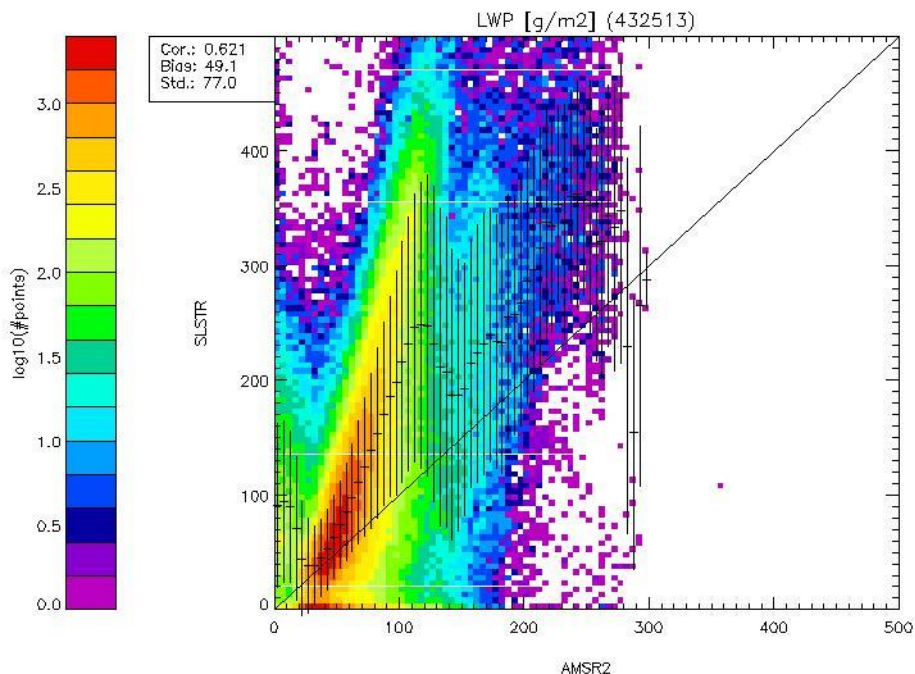


**Figure 3-1** 2d-frequency distribution and validation scores for Cloud\_cci SLSTR-A and SLSTR-B v3 cloud liquid water path (LWP) using AMSR2 as reference. Collocation time window: 15 minutes. All Cloud\_cci data within an AMSR2 footprint were averaged.

### 3.2 Level-3 data

#### 3.2.1 Comparisons with SEVIRI data

In this section we compare the Cloud\_cci SLSTR S3A and S3B v3 products with Cloud\_cci SEVIRI v3, using L3 monthly data. There is no substantial differences between S3B or S3A in comparison with SEVIRI (see Table 3-1). Thus graphics are only shown for July 2019 S3A.

L3 data from SLSTR are averages of satellite morning overpass while SEVIRI L3 are obtained with all day measurements. Differences, when comparing these L3 dataset, can be due to daily cycle as well as different observation geometry (as longer optical path going toward the edge of SEVIRI disk) and different sensitivity.

Figures 3-2 to 3-5 show examples of comparisons, for different cloud products, between SEVIRI and SLSTR-A for the month February 2019. Table 3-1 summarize the comparison in term of mean and biases for the cloud product considering the common region (SEVIRI disk) for both instruments.

Cloud fraction (CFC) present ocean/land discontinuity that is mainly coming from the ocean land discontinuity in low cloud fraction (CFC\_low). SLSTR present lower fraction of low cloud over land and a more general lower fraction of high cloud, this is reflected in an average lower CTH (with bias average value around 1km). SEVIRI show higher total cloud fraction over land and at the edge of SEVIRI disk. COT differences tend to increase toward the edge of SEVIRI disk and SEVIRI CER is higher toward the edge of the disk that may be explained with longer SEVIRI optical path and consequently different sensitivity. Locally there are differences up to 20% in liquid cloud fraction when in average the bias is no more than 3%. Difference in cloud phase could be responsible in difference in retrieved cloud properties and IWP and LWP.

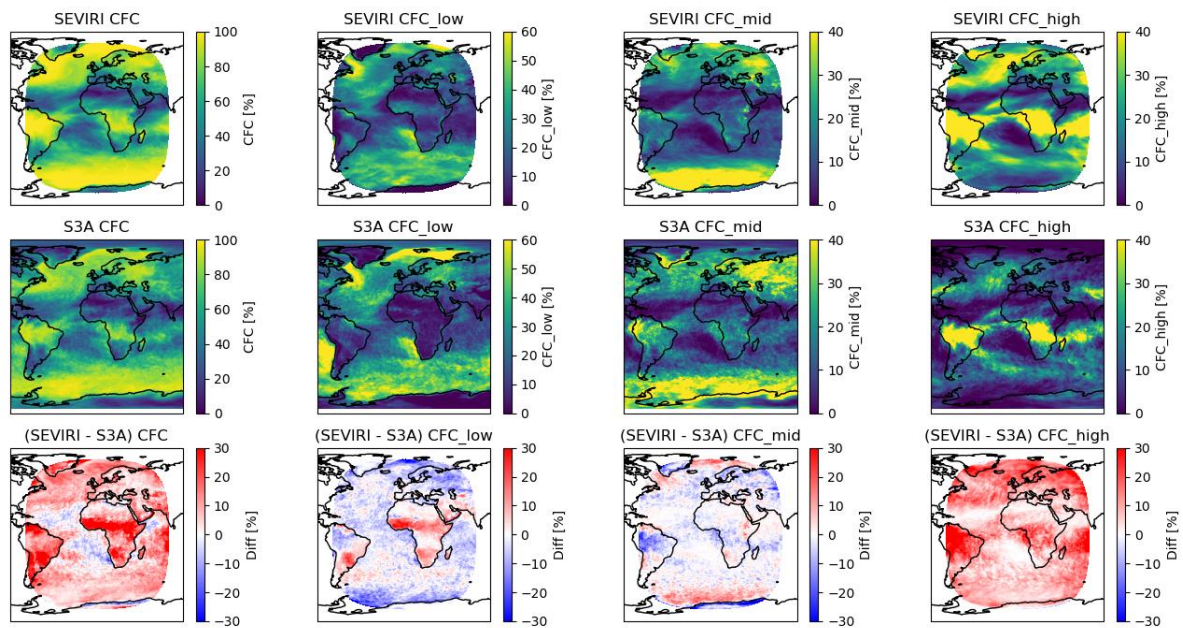


**Figure 3-2** Cloud fraction (CFC) monthly mean for February 2019. Top row: SEVIRI total cloud fraction, low cloud fraction, middle and high cloud fraction. Middle row: SLSTR-A total cloud fraction, low, middle and high cloud fraction. Bottom row show the differences SEVIRI-SLSTR-A for total, low, middle and high cloud fraction.



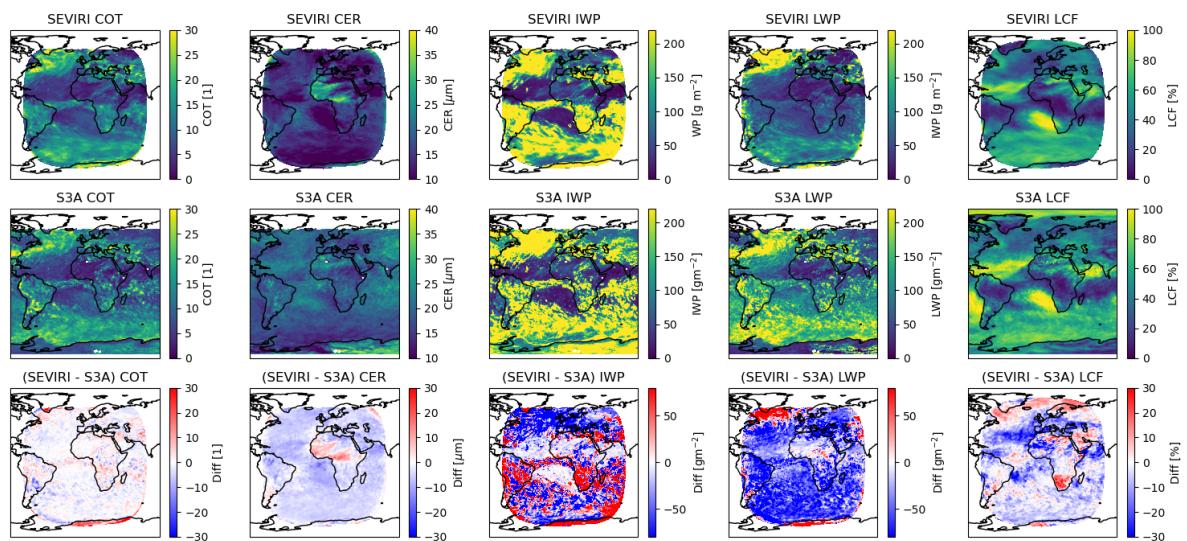


**Figure 3-3** Monthly mean (February 2019) maps of: Cloud Optical thickness (COT), Cloud effective radius (CER), Ice water Path (IWP), liquid Water Path (LWP) and liquid cloud fraction (LCF). Top row: SEVIRI, middle row: SLSTR-A, bottom row: differences SEVIRI-SLSTR-A.

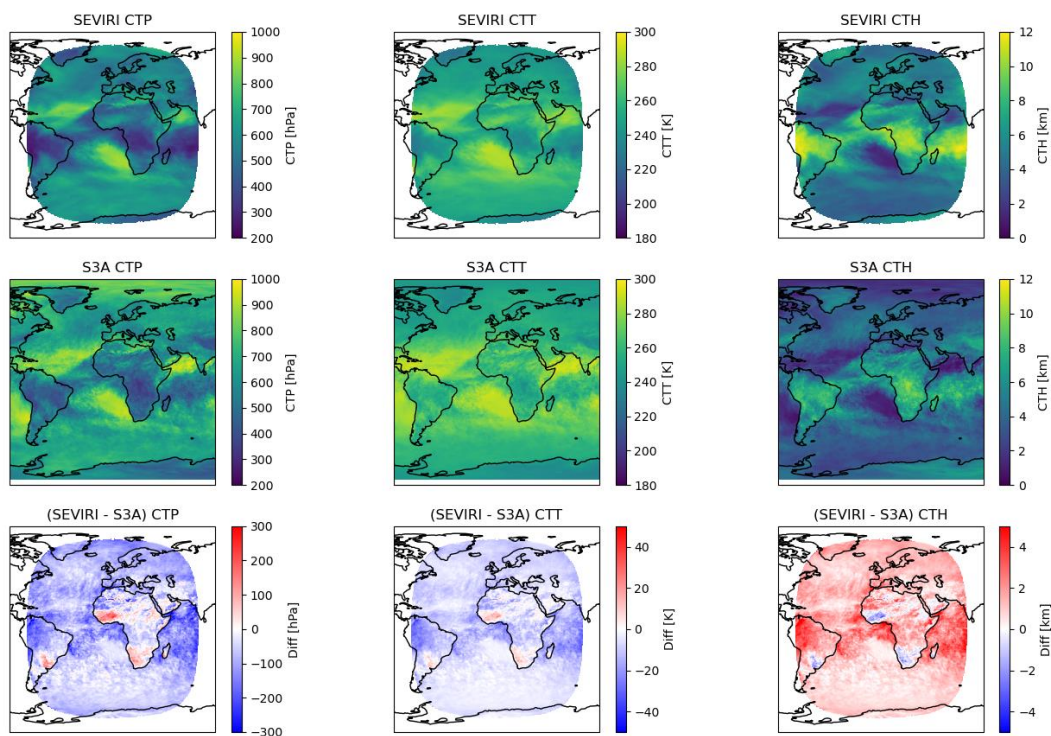


**Figure 3-4** Monthly mean (February 2019) maps of: Cloud Top Pressure (CTP), Cloud Top Temperature (CTT), Cloud Top High (CTH). Top row: SEVIRI, middle row: SLSTR-A, bottom row: differences SEVIRI-SLSTR-A.

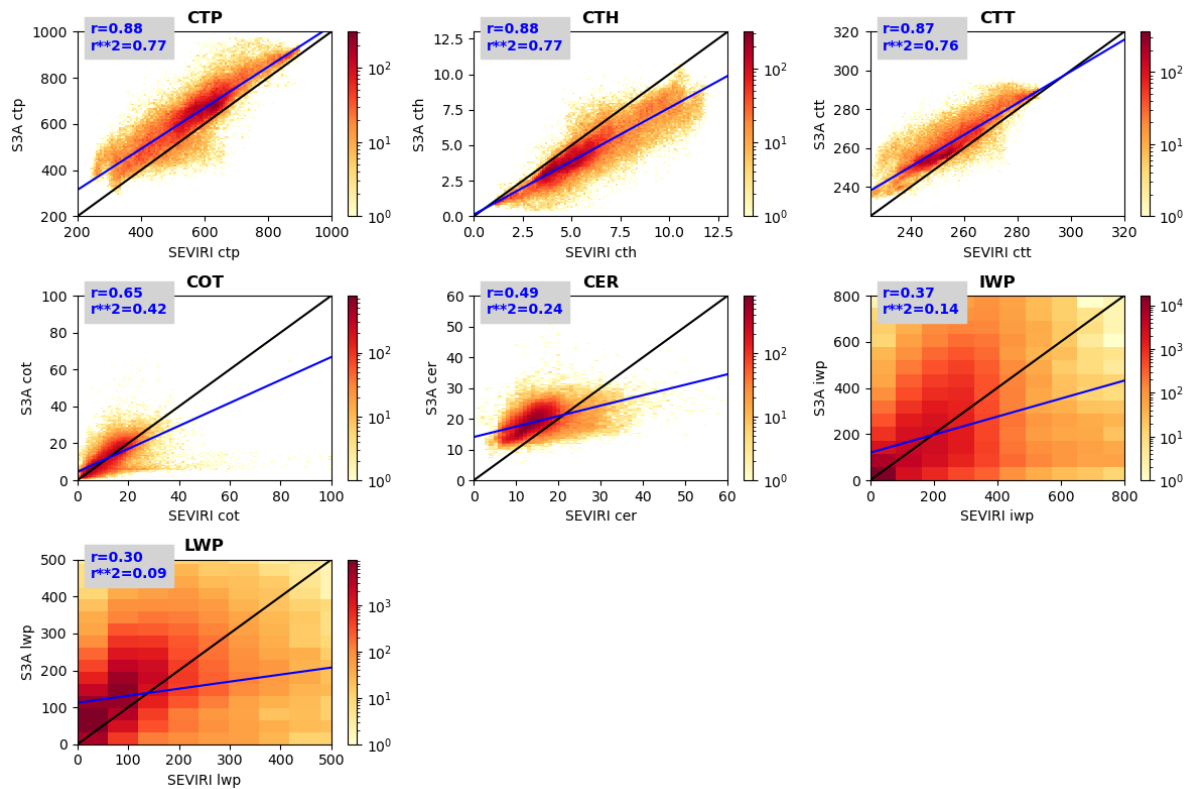


Figure 3-5 Density scatter plot with correlation ( $r$ ) between SLSTR S3a and SEVIRI for February 2019.


Table 3-1 Summary of Level-3 comparison of SEVIRI cloud products with SLSTR-A (S3A) and SLSTR-B (S3B) for the months February 2019.

Variable	SEVIRI mean	S3A mean	Bias (SEVIRI-S3A)	S3B mean	Bias (SEVIRI-S3B)
CFC [%]	69.8	60.5	9.3	59.8	9.9
CFC_low [%]	24.6	26.9	-2.3	26.6	-1.9
CFC_mid [%]	18.0	19.0	-1.0	18.7	-0.6
CFC_high [%]	24.2	13.3	10.9	13.5	10.7
CTP [mb]	565.6	638.9	-73.3	638.2	-72.6
CTT [K]	254.9	262.6	-7.7	262.5	-7.6
CTH [km]	5.6	4.3	1.3	4.4	1.3
COT	12.3	12.2	0.07	12.8	-0.5
CER [ $\mu\text{m}$ ]	14.8	19.1	-4.2	19.1	-4.2
IWP [ $\text{g}/\text{m}^2$ ]	180.8	190.0	-9.0	194.2	-13.3
LWP [ $\text{g}/\text{m}^2$ ]	94.3	129.9	-36.1	150.4	-56.2
LCF [%]	45.1	49.7	-4.5	48.6	-3.5

### 3.2.2 Comparison with MODIS collection 6

In this section Cloud\_cci SLSTR v3 L3C products from S3A and S3B are compared between them-self and with MODIS cloud collection 6.1 products in term of: global maps, differences, scatter density plot with estimate of correlation coefficient and biases.

Figures 3-6 to 3-11 show maps and scatter plots for different cloud parameters for the months of February and July 2019. Table 3-2 collects mean the biases and correlation considering all months of 2019. Note that both scatter plots and values in Table 3-2 are obtained using all latitude range. Cloud Fraction (CFC) is generally higher in MODIS data then SLSTR with exception of Antarctica, global bias (for both instruments and all months considered), is less than 10% cloud fraction with good

	<b>Doc:</b>		Cloud_cci+_D4.1_PVIR_v3.0.docx		
	<b>Date:</b>		20.11.2023		
	<b>Issue:</b>	3	<b>Revision:</b>	0	Page 35

correlation (0.88 and higher). Prominent region with increased biases are Tropical Atlantic and Indian Ocean as well as Eastern Asia.

Clout top height shows good correlation with MODIS (0.83 and higher) and global bias of 0.15 km or lower, but SLSTR height tend to be lower than MODIS in particular for higher clouds (where monthly mean higher than 6 km).

COT maps present increasing differences at higher latitudes. Scatter plots show higher values for MODIS COT, in particular SLSTR present lower values for MODIS COT higher than 20.

Differences in IWP between MODIS and SLSTR are relatively small with a small tendency to higher values in MODIS data over land and at higher latitudes.

LWP maps show generally higher LWP in SLSTR over ocean while quite some land regions are characterized by lower LWP values in SLSTR compared to MODIS. LWP scatter plots show low bias and good correlation with MODIS for low LWP, but values tend to depart from each other for higher LWP, in particular for MODIS LWP higher than 200 g/m<sup>2</sup> and altogether it results in correlation values between 0.1 and 0.5.

There are different reasons that may explain why LWP from MODIS and SLSTR differ more at high latitude toward the poles. The LWP estimate are dependent on the shortwave channels and are affected by ice/snow identification and sea ice mask detection problems. MODIS is also known to overestimate LWP at high latitude: Sheethala et al (2010) link the MODIS overestimation to the solar zenith angles and find that the differences between MODIS LWP and AMSR-E LWP increase for heterogeneous cloud at low Sun.

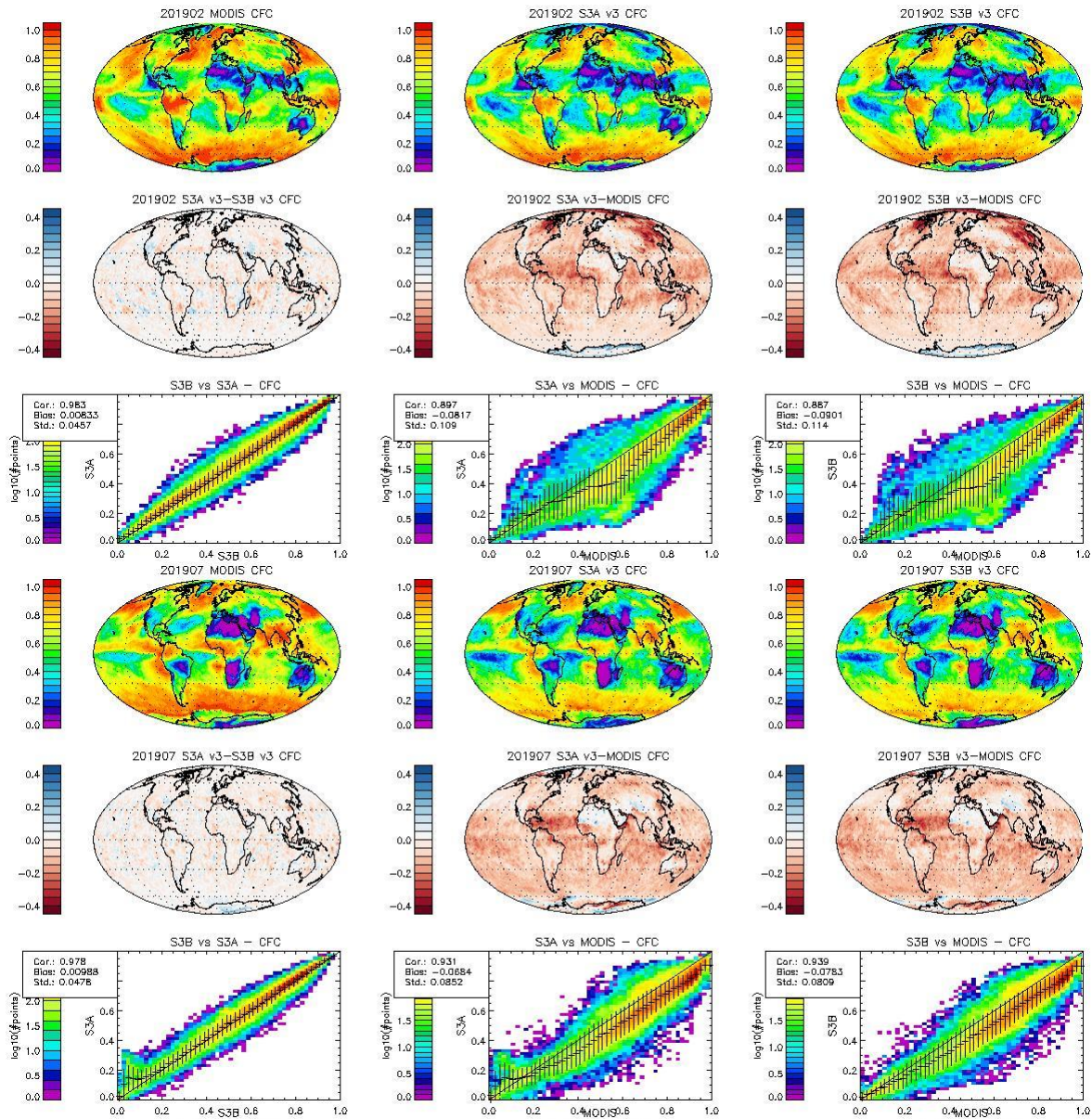


**Figure 3-6** Monthly mean cloud fraction for February (first 3 rows) and July 2019 (last 3 rows); First row show CFC mean for MODIS, SLSTR-A (S3A) and SLSTR-B (S3B); second row show the differences: S3A-S3B, S3A-MODIS, S3B-MODIS; Third row show the density scatter plot between: S3A vs S3B, S3A vs MODIS and S3B vs MODIS;

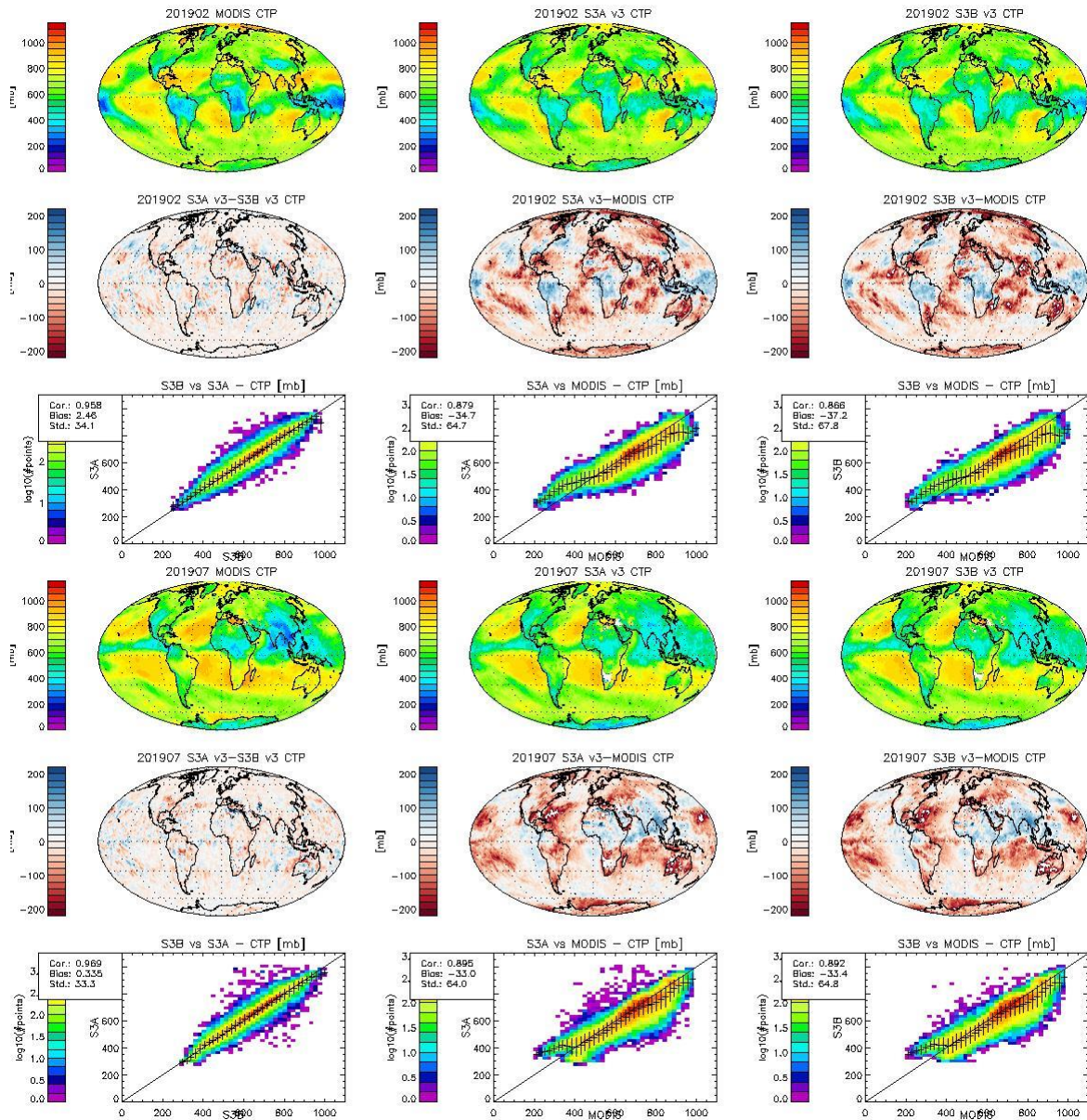


**Figure 3-7** Monthly mean cloud top pressure (CTP) for February (first 3 rows) and July 2019 (last 3 rows); First row show CTP mean for MODIS, SLSTR-A (S3A) and SLSTR-B (S3B); second row show the differences: S3A-S3B, S3A-MODIS, S3B-MODIS; Third row show the density scatter plot between: S3A vs S3B, S3A vs MODIS and S3B vs MODIS;

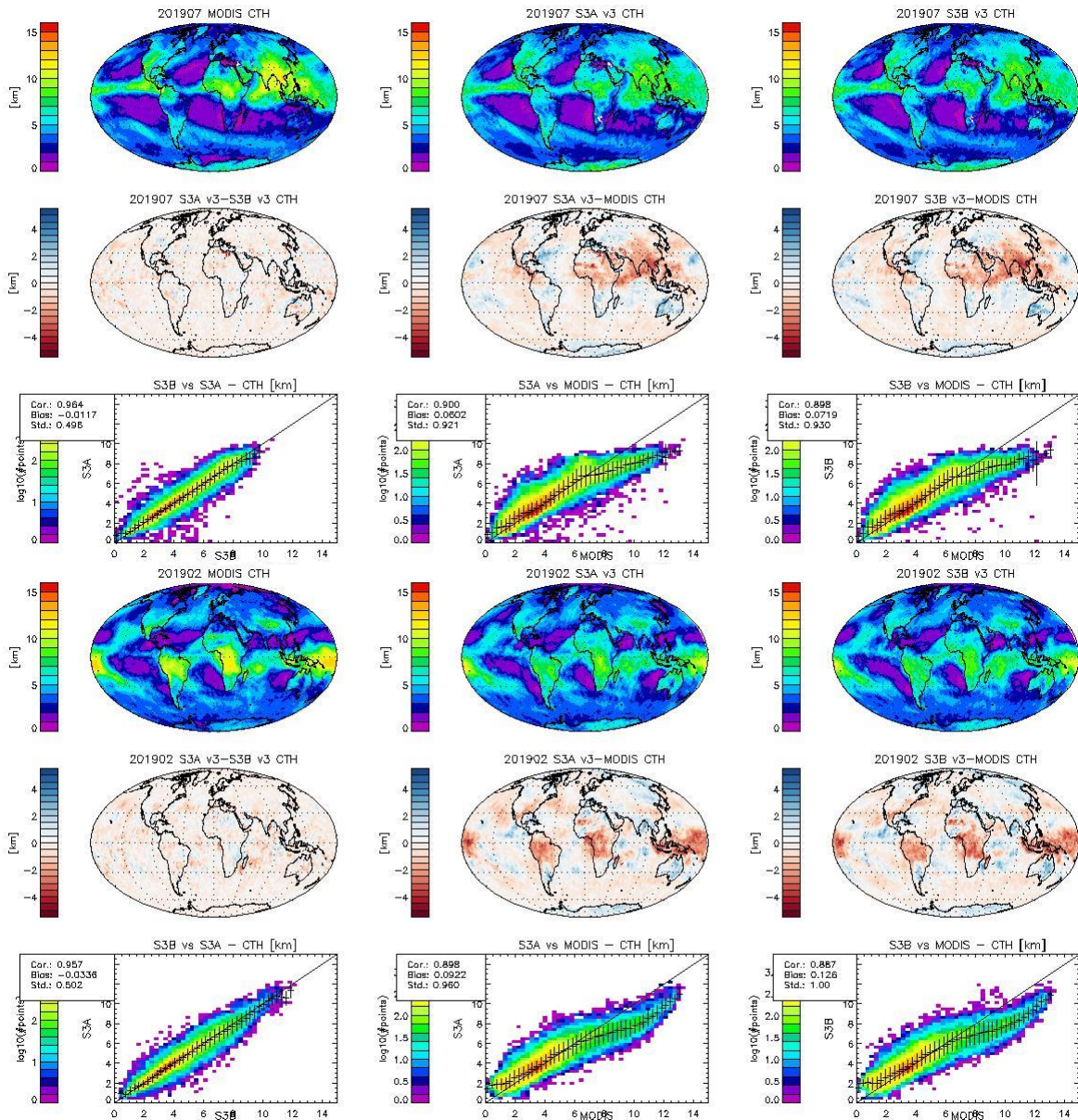


**Figure 3-8** Monthly mean Cloud Top Height (CTH) for February (first 3 row) and July 2019 (last 3 row); First row show CTH mean for MODIS, SLSTR-A (S3A) and SLSTR-B (S3B); second row show the differences: S3A-S3B, S3A-MODIS, S3B-MODIS; Third row show the density scatter plot between: S3A vs S3B, S3A vs MODIS and S3B vs MODIS

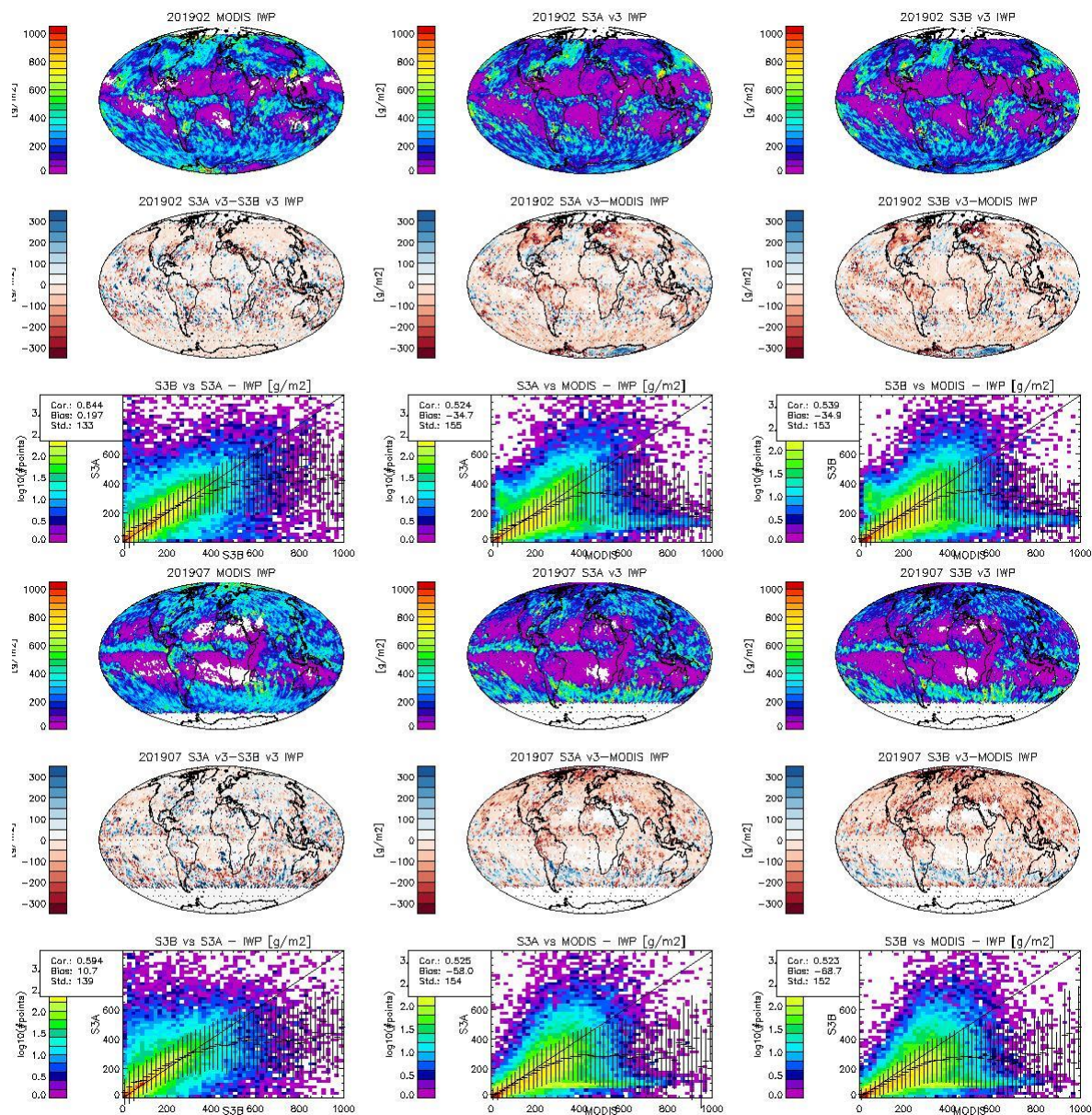


**Figure 3-9** Monthly mean Ice Water Path (IWP) for February (first 3 row) and July 2019 (last 3 row); First row show IWP mean for MODIS, SLSTR-A (S3A) and SLSTR-B (S3B); second row show the differences: S3A-S3B, S3A-MODIS, S3B-MODIS; Third row show the density scatter plot between: S3A vs S3B, S3A vs MODIS and S3B vs MODIS;

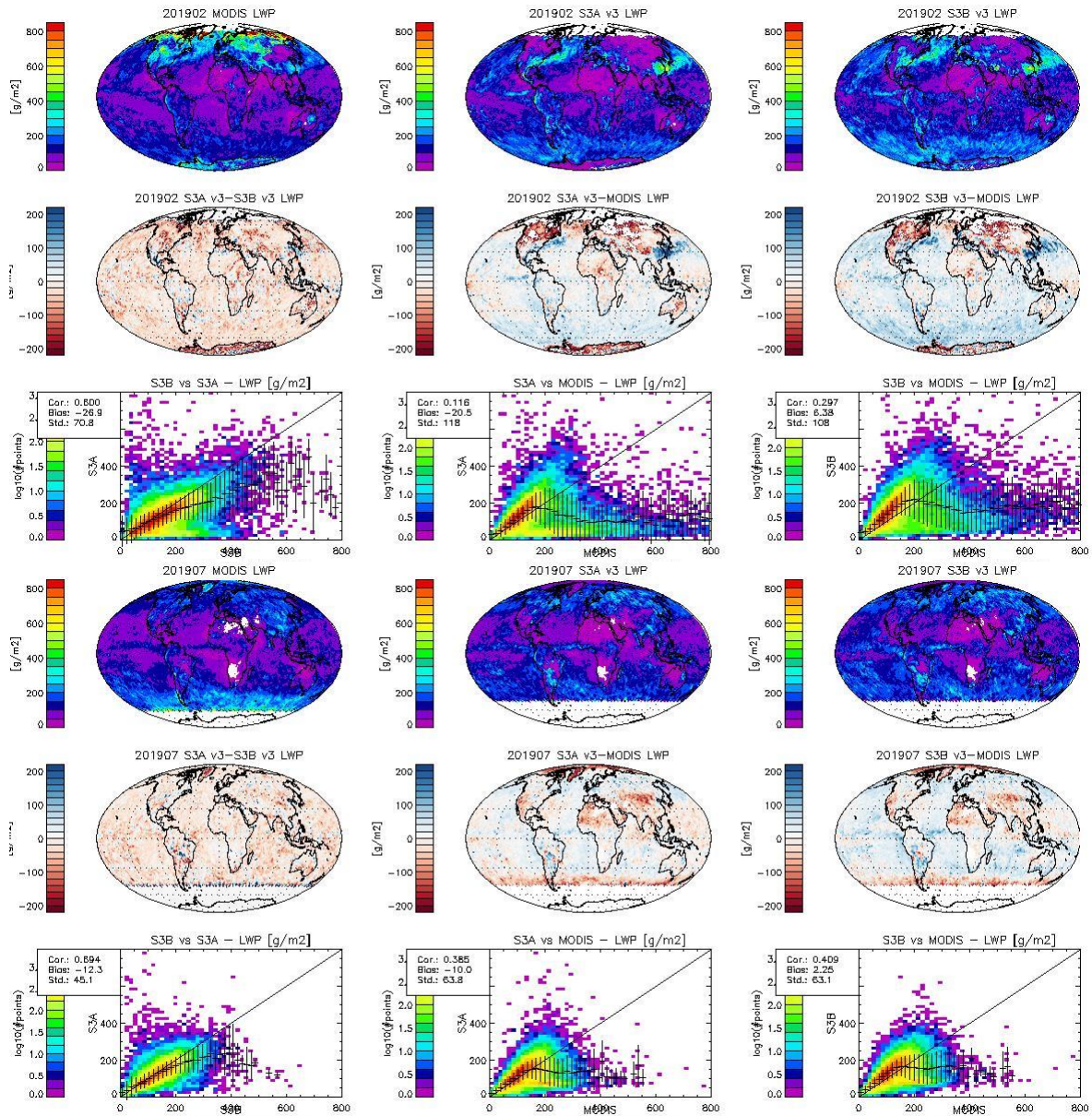


**Figure 3-10** Monthly mean Liquid Water Path (LWP) for February (first 3 lines) and July 2019 (last 3 lines); First row show CFC mean for MODIS, SLSTR-A (S3A) and SLSTR-B (S3B); second row show the differences: S3A-S3B, S3A-MODIS, S3B-MODIS; Third row show the density scatter plot between: S3A vs S3B, S3A vs MODIS and S3B vs MODIS;



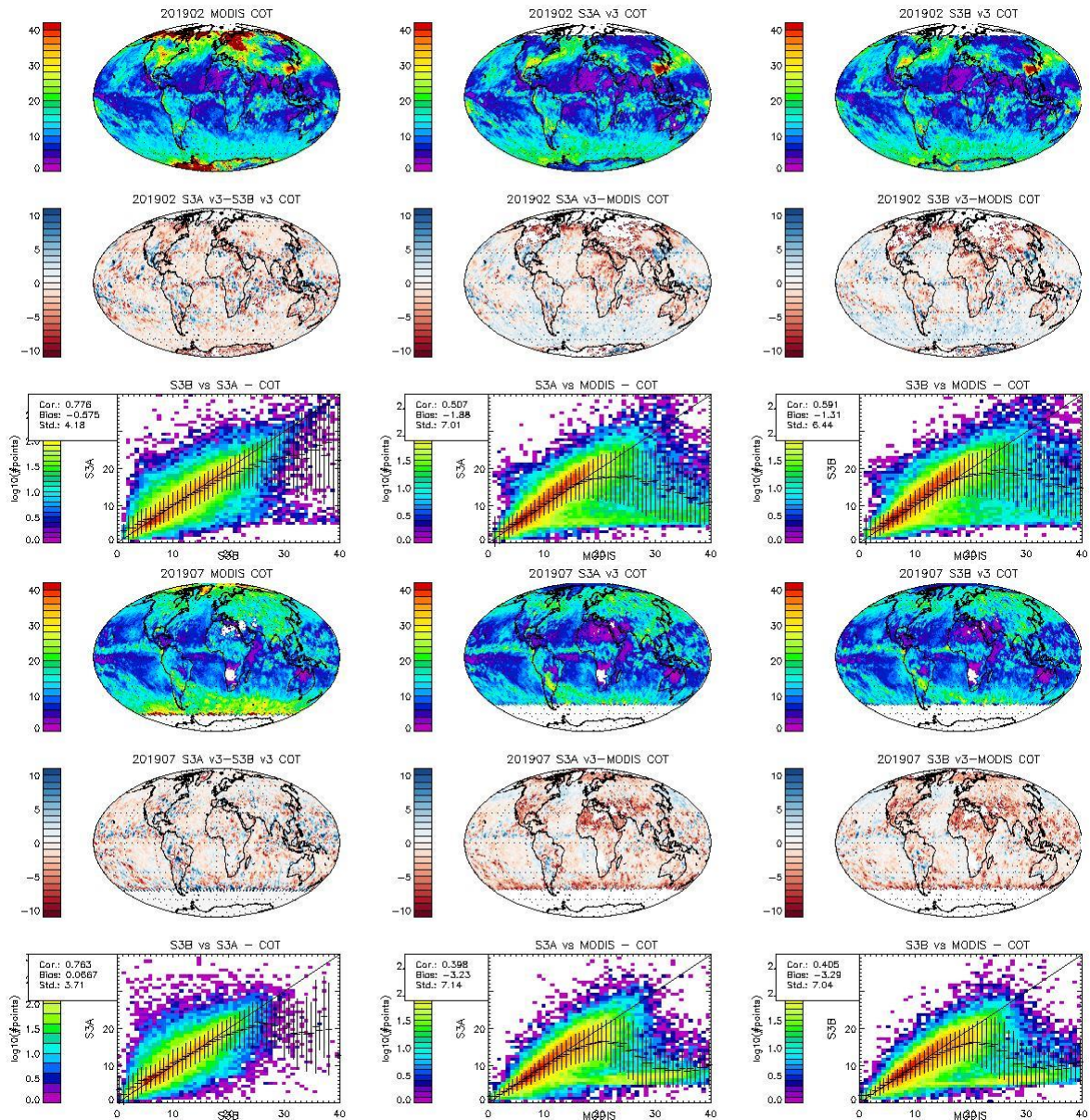


**Figure 3-11** Monthly mean Cloud Optical Thickness (COT) for February (first 3 lines) and July 2019 (last 3 lines); First row show COT mean for MODIS, SLSTR-A (S3A) and SLSTR-B (S3B); second row show the differences: S3A-S3B, S3A-MODIS, S3B-MODIS; Third row show the density scatter plot between: S3A vs S3B, S3A vs MODIS and S3B vs MODIS;

**Table 3-2 Summary of Level-3 comparison of MODIS cloud products with SLSTR-A (S3A) and SLSTR-B (S3B) considering all months of 2019. The biases and correlation reported here are the mean of the 12 monthly comparison.**

Variable	Global Bias - S3A-S3B [Feb./July.]	Global Bias S3A-MODIS	Global Bias S3B-MODIS
CFC [% 0-1]	0.01	0.07	0.08
CTP [mb]	0.8	-36	-37
CTH [km]	-0.01	0.10	0.11
IWP [g/m <sup>2</sup> ]	8.1	-46	-54
LWP [g/m <sup>2</sup> ]	-21	-18	2.2
COT	-0.25	-2.53	-2.28
Variable	Global corr. coeff S3A-S3B	Global c. c. S3A-MODIS	Global cc S3B-MODIS
CFC	0.97	0.92	0.93
CTP	0.95	0.87	0.86
CTH	0.94	0.89	0.88
IWP	0.60	0.51	0.51
LWP	0.63	0.27	0.40
COT	0.72	0.50	0.54

### 3.2.3 Validation of SLSTR Level-3 radiative fluxes with CERES and BSRN

#### CERES

In this section the Top of Atmosphere (TOA) upwelling shortwave and longwave radiation from SLSTR are compared against Clouds and Earth Radiation Energy System (CERES) Energy Balanced and Filled (EBAF) fluxes Edition 4.1 Top of atmosphere (TOA) fluxes Edition (see Section A.6)

Figures 3-12 and 3-13 show, as example, the TOA maps for February 2019 for SLSTR-A and B together with CERES and the difference (SLSTR-CERES).

The maps of clear sky radiations identify the effects that are not due to clouds but due to differences in: surface reflectance (shortwave), surface emissivity and temperature (longwave), atmospheric profiles and radiative transfer. An additional aspect is the diurnal cycle correction for the imperfect sampling of the diurnal cycle, which is done differently in Cloud\_cci and CERES. Over ocean both longwave and shortwave clear sky radiation are underestimated; over land there are regions where shortwave fluxes are overestimated, in particular in mountain and snow covered regions and deserts. We can identify some snow/ice area (especially in SLSTR-B) as Greenland and Antarctica edges where SLSTR underestimate shortwave fluxes.

Maps of all sky fluxes show overestimation of shortwave fluxes over South hemisphere (that don't have a corresponding feature on longwave fluxes), that could be explained with overestimation of low level clouds, or again be due to differences in diurnal cycle corrections.

Figures 3-14 and 3-15 show the density scatter plot of SLSTR fluxes (A and B respectively) vs. CERES, including data from both months February and July 2019 data.

Very good correlations, all above 0.97, are found with small shortwave biases below 6 W/m<sup>2</sup> for both SLSTR A and B, and longwave biases of -0.19 and 0.06 W/m<sup>2</sup>.

Table 3-4 lists the standard deviations and biases against CERES stratified by USGS surface type. For shortwave regions with little or none vegetation show highest errors values, while for longwave the values for standard deviation and bias are smaller on average.

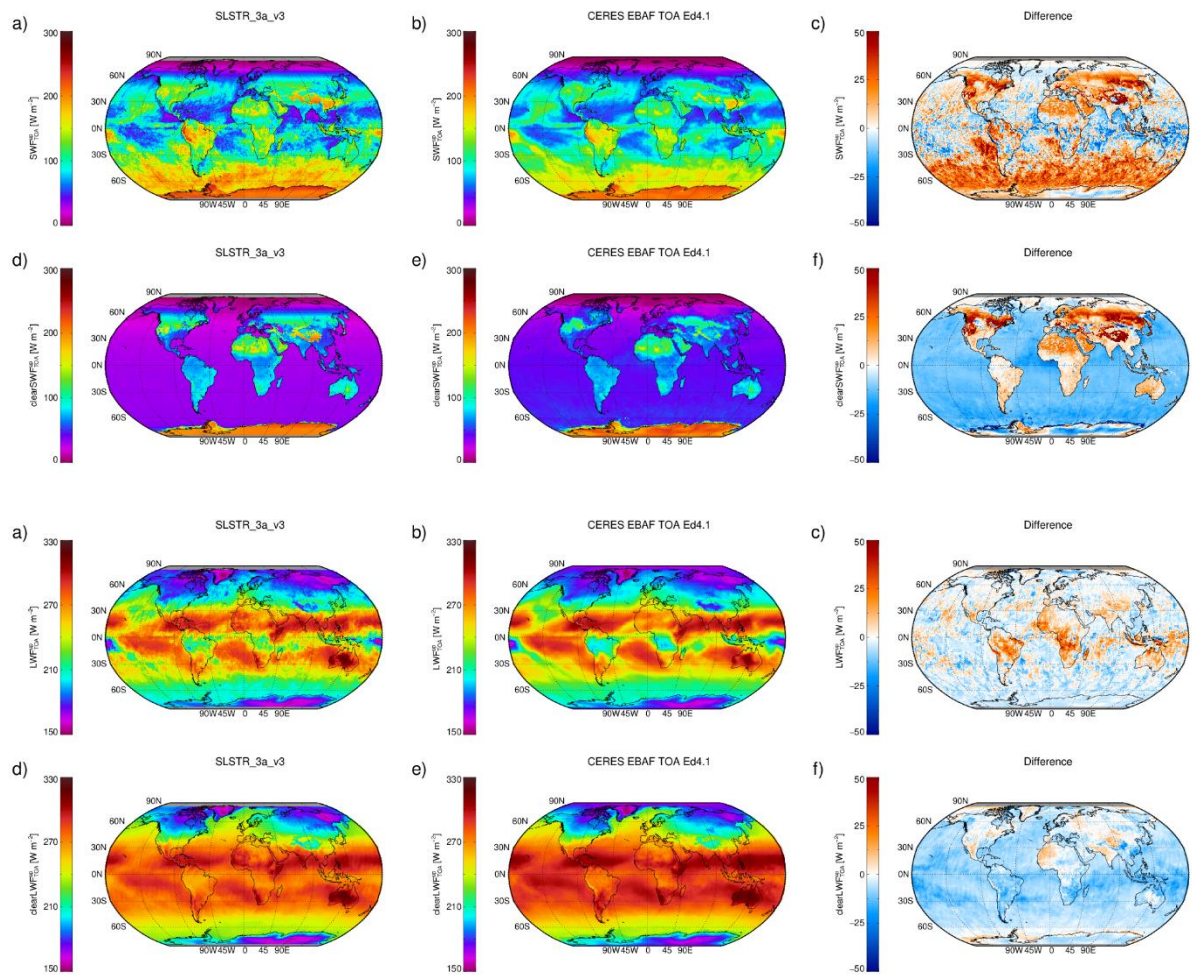


**Figure 3-12** Monthly mean maps of TOA radiations for Feb 2019. First row shows all sky shortwave flux for SLSTR-A; CERES and the difference (SLSTR-CERES). Second row shows clear sky shortwave flux for: SLSTR-A; CERES and the difference. Third row shows longwave all sky longwave flux for: SLSTR-A; CERES and the difference. Fourth row shows longwave clear sky flux for: SLSTR-A; CERES and the difference.

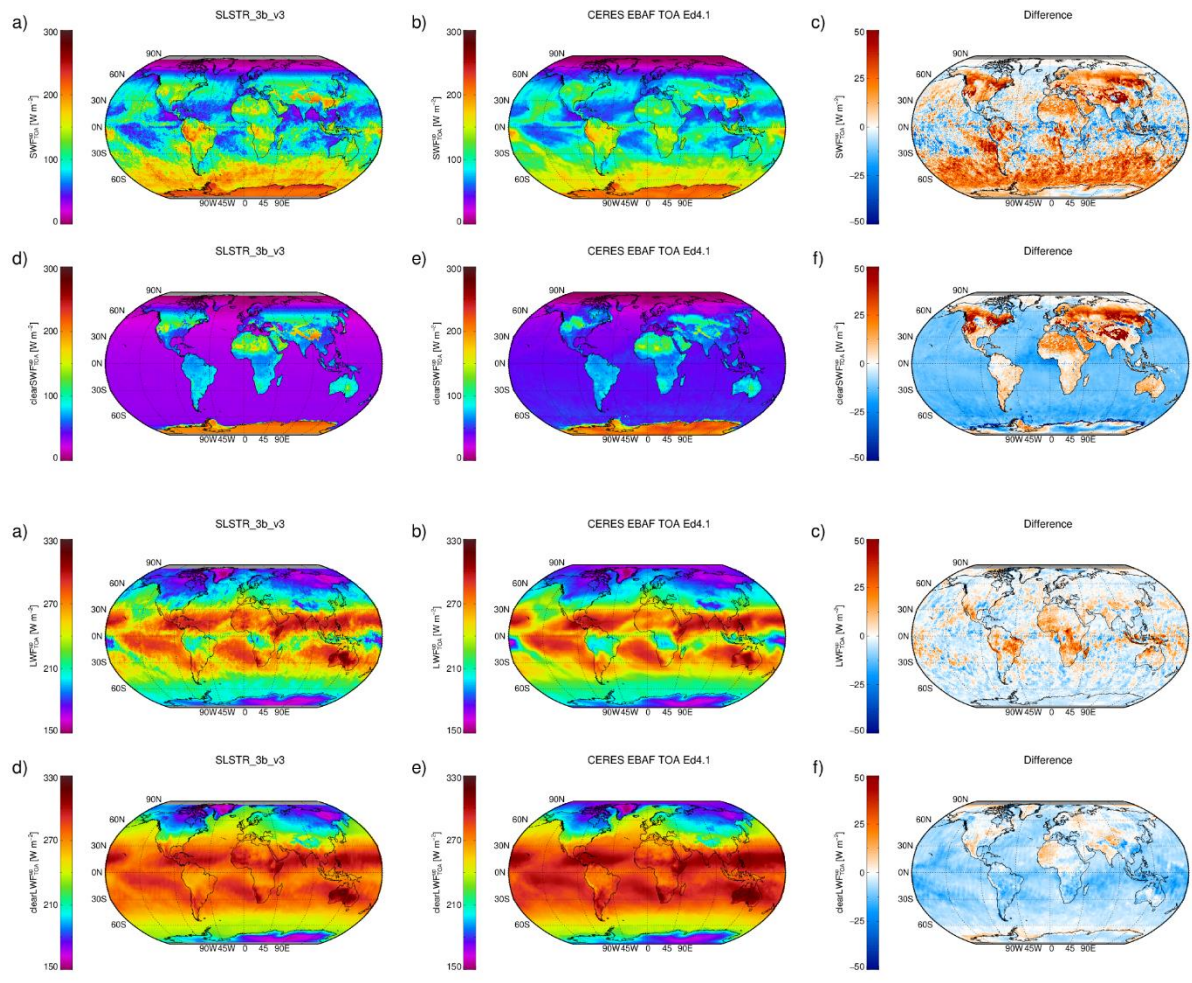


**Figure 3-13** Monthly mean maps of TOA radiations for Feb 2019. First row shows all sky shortwave flux for SLSTR-B; CERES and the difference (SLSTR-CERES). Second row shows clear sky shortwave flux for: SLSTR-B; CERES and the difference. Third row shows longwave all sky longwave flux for: SLSTR-B; CERES and the difference. Fourth row shows longwave clear sky flux for: SLSTR-B; CERES and the difference.

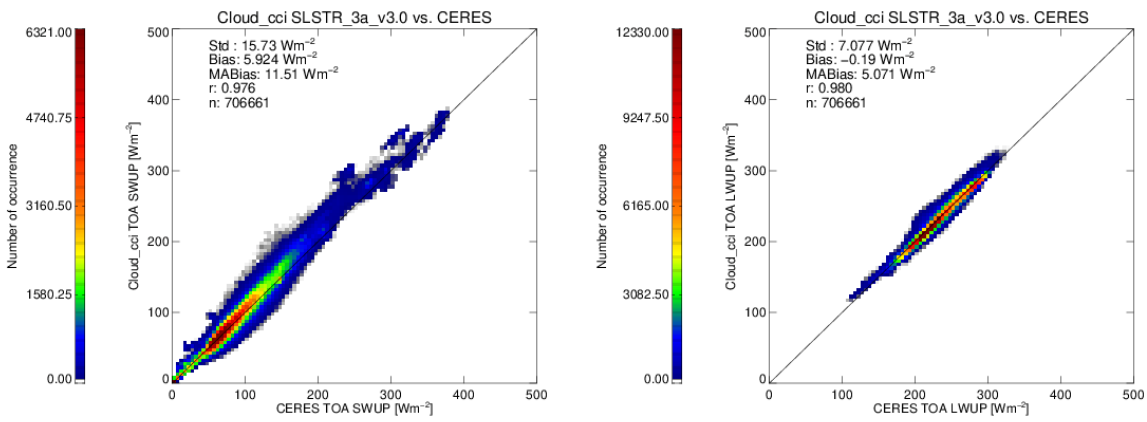


**Figure 3-14** Density scatter plot of SLSTR S3a vs CERES EBAF-TOA Ed4.0 top of atmosphere (TOA) monthly mean upwelling shortwave (left) / longwave (right) flux for 2019.

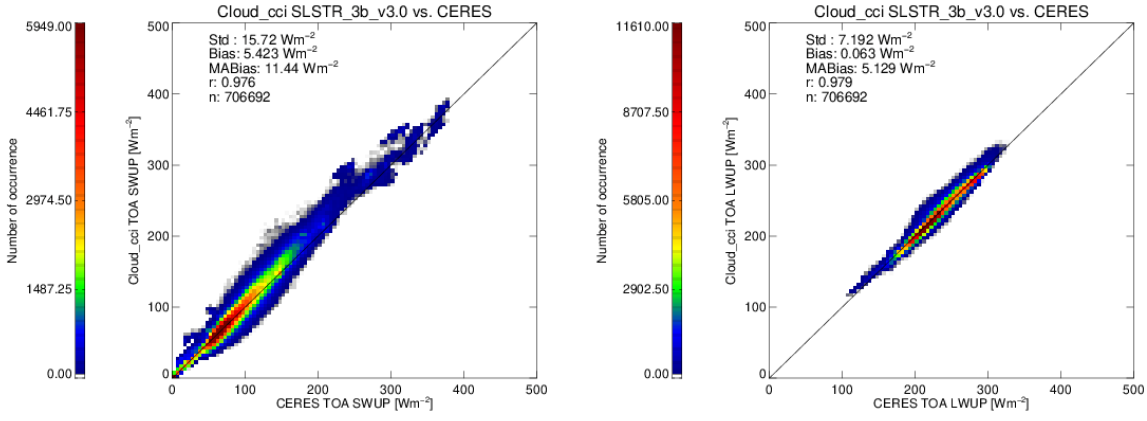


**Figure 3-15** Density scatter plot of SLSTR S3b vs CERES EBAF-TOA Ed4.0 top of atmosphere (TOA) monthly mean upwelling shortwave (left) / longwave (right) flux for 2019.

**Table 3-3** *Cloud\_cci SLSTR S3a v3 top of atmosphere (TOA) monthly mean upwelling shortwave flux validation against to CERES EBAF-TOA Ed4.0 stratified by USGS surface type. Data basis contains monthly mean data including all months in 2019.*

USGS class	TOA <sub>up</sub> shortwave flux		TOA <sub>up</sub> longwave flux	
	Bias [Wm <sup>-2</sup> ]	Std [Wm <sup>-2</sup> ]	Bias [Wm <sup>-2</sup> ]	Std [Wm <sup>-2</sup> ]
Water	4.32878	14.5504	-1.40583	6.02280
Evergreen Needle leaf Forest	16.3356	23.9670	-0.0149349	4.52107
Evergreen Broadleaf Forest	5.89291	15.0829	9.10287	11.5240
	16.3319	22.6144	-0.233566	3.33716
Deciduous Broadleaf Forest	8.65984	13.9615	1.02528	7.07559
Mixed Forests	14.9411	22.8138	-0.264130	4.99942
Closed Shrublands	5.25652	16.1396	4.58986	10.7101
Open Shrublands	7.92915	14.7864	2.11319	7.42567
Woody Savannas	7.66896	17.8605	4.20869	9.77815
Savannas	3.92271	13.8732	6.25604	10.2701
Grasslands	11.0836	21.3496	2.97664	7.49260
Permanent Wetland	8.45961	17.3373	1.17889	6.97250
Croplands	6.91605	12.2050	3.06651	7.74202
Urban and Built-Up	5.69802	15.4342	2.15425	7.68370
Cropland/Natural Vegetation Mosaic	6.88322	15.1067	4.37681	9.43474
Snow and Ice	8.63588	16.9582	-1.58891	5.98913
Barren or Sparsely Vegetated	16.1608	15.8582	6.51607	8.25822

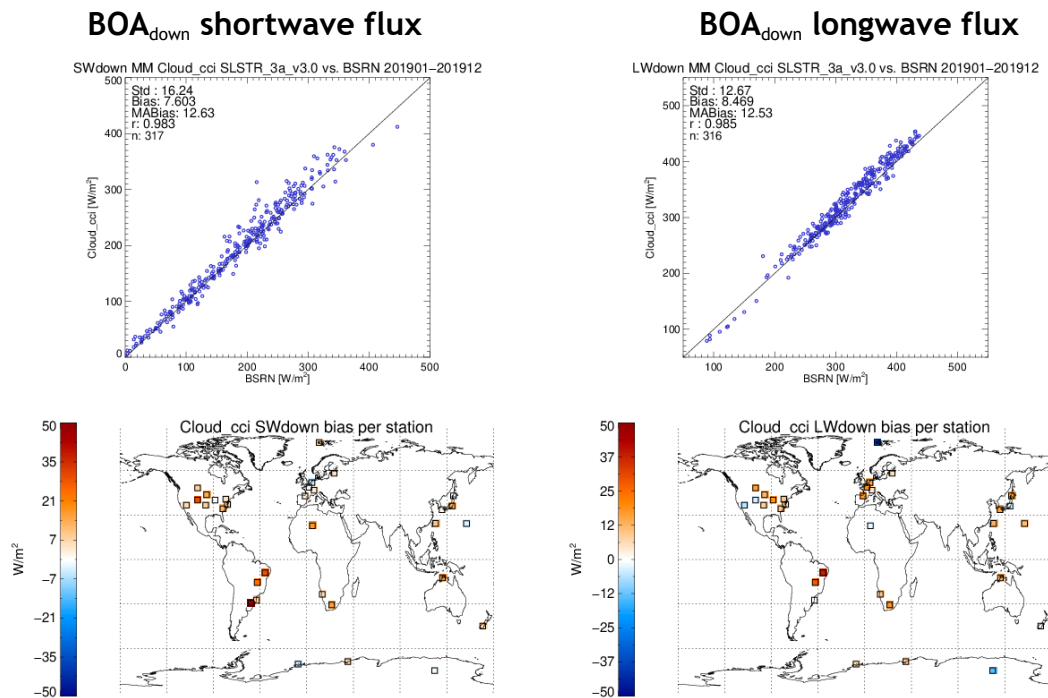
**Table 3-4** *Cloud\_cci SLSTR S3b v3 top of atmosphere (TOA) monthly mean upwelling shortwave flux validation against to CERES EBAF-TOA Ed4.0 stratified by USGS surface type. Data basis contains monthly mean data including all months in 2019.*

USGS class	TOA <sub>up</sub> shortwave flux		TOA <sub>up</sub> longwave flux	
	Bias [Wm <sup>-2</sup> ]	Std [Wm <sup>-2</sup> ]	Bias [Wm <sup>-2</sup> ]	Std [Wm <sup>-2</sup> ]
Water	3.63072	14.4637	-1.10992	6.14447
Evergreen Needle leaf Forest	15.8913	23.5988	0.242545	4.44113
Evergreen Broadleaf Forest	5.69172	15.3132	9.13007	11.5226
	15.6748	21.9060	0.124527	3.56635
Deciduous Broadleaf Forest	7.36052	14.4667	1.52932	8.01868
Mixed Forests	14.1460	22.5797	0.124501	5.26153
Closed Shrublands	2.81216	15.0102	6.90583	11.6072
Open Shrublands	7.88019	14.6558	2.44414	7.76389
Woody Savannas	7.17937	17.5537	4.31991	9.66424
Savannas	2.94206	13.6380	6.78126	10.3606
Grasslands	11.1947	21.3297	3.19595	7.70281
Permanent Wetland	8.04975	16.7905	1.34033	6.84512
Croplands	6.32803	12.5193	3.44738	7.90109
Urban and Built-Up	4.82376	14.9897	2.55768	7.71600
Cropland/Natural Vegetation Mosaic	6.17618	15.0928	4.76595	9.29982
Snow and Ice	9.52190	17.2188	-1.77006	6.11771
Barren or Sparsely Vegetated	16.2058	15.9234	6.63298	8.46349

**BSRN**

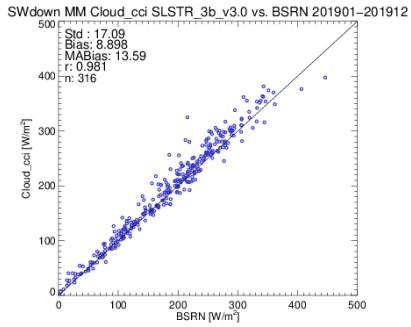
BSRN stations measure direct, diffuse and global downwelling shortwave and longwave fluxes in 1 min temporal resolution. The manned stations are located at positions, which are representative of a relatively large surrounding area for the use in satellite data validation among others. The 1-min data was aggregated to monthly averages which were used as validation data.

Figure 3-16 and Figure 3-17 shows scatter plots and validation scores, for monthly mean BOA downwelling shortwave and longwave radiation, for SLSTR-A and B respectively. Shortwave standard deviations lie between 16 and 17 W/m<sup>2</sup> for both satellites, and biases range from 7 to 9 W/m<sup>2</sup>. Longwave standard deviation lie around 13 W/m<sup>2</sup> for both satellites and biases are 8.5 W/m<sup>2</sup> and 9.7 W/m<sup>2</sup> for S3B and S3A respectively. Correlations are very high and above 0.98 for both instruments and spectral ranges. The shown bias maps reveal a rather uniform performance over all stations, with the majority of stations that show a positive bias, e.g. satellite estimate higher downwelling fluxes then ground measurements.



**Figure 3-16** Cloud\_cci SLSTR S3a bottom of atmosphere (BOA) monthly mean downwelling shortwave flux validation (left) and downwelling longwave flux (right) against to BSRN. Data basis contains monthly mean data for all months in 2019.

### BOA<sub>down</sub> shortwave flux




### BOA<sub>down</sub> longwave flux

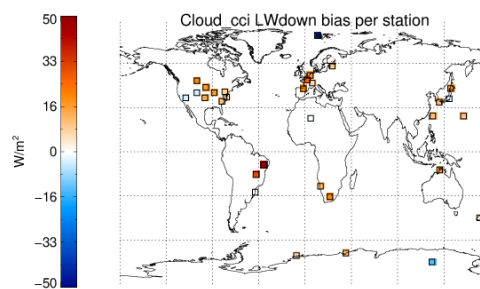
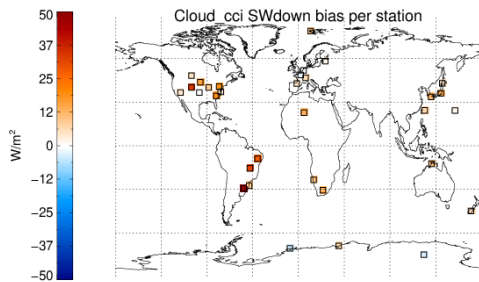
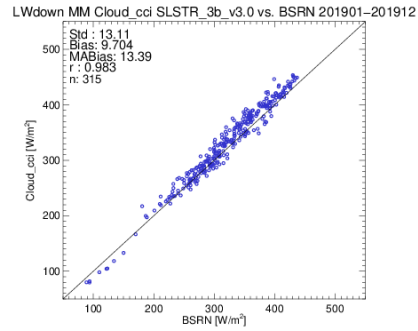


**Figure 3-17** *Cloud\_cci SLSTR S3b bottom of atmosphere (BOA) monthly mean downwelling shortwave flux validation (left) and downwelling longwave flux (right) against to BSRN. Data basis contains monthly mean data for all months 2019.*



	<b>Doc:</b>		Cloud_cci+_D4.1_PVIR_v3.0.docx		
	<b>Date:</b>		20.11.2023		
	<b>Issue:</b>	3	<b>Revision:</b>	0	Page 49


## 4 Summary

This report summarizes the validation result for version 3 of Cloud\_cci SEVIRI and SLSTR demonstrator datasets generated in Cloud\_cci+ Phase I. The data comprises all months in 2019 and the validation results highlight the good quality of this third and final demonstrator versions with many improvements over the first version.

## 5 Definitions, Acronyms, Abbreviations


AATSR	Advanced Along Track Scanning Radiometer
ATBD	Algorithm Theoretical Basis Document
ATSR	Along-Track Scanning Radiometer
AVHRR	Advanced Very High Resolution Radiometer
CEDA	British Atmospheric Data Centre
BRDF	Bidirectional Reflectance Distribution Function
CALIPSO	Cloud-Aerosol Lidar and Infrared Pathfinder Satellite Observations
CFMIP	Cloud Feedback Model Intercomparison Project
CM	Configuration Management
CMIP	Climate Model Intercomparison Project
CM SAF	EUMETSAT Satellite Application Facility on Climate Monitoring
COSP	CFMIP Observational Simulator Package
DARDAR	raDAR/liDAR
DISORT	Discrete Ordinates Radiative Transfer
DWD	Deutscher Wetterdienst
EC-EARTH	Earth system climate modelling version of the ECMWF model
ECMWF	European Centre for Medium Range Weather Forecast
ECSS	European Cooperation for Space Standardization
ECV	Essential Climate Variable
EO	Earth Observation
EOS	Earth Observing System
ESA	European Space Agency
EUMETSAT	European Organization for the Exploitation of Meteorological Satellites
FCDR	Fundamental Climate Data Record
GCM	Global Circulation Model
GCOS	Global Climate Observing System
GERB	Geostationary Earth Observation Budget Instrument
GEWEX	Global Energy and Water Cycle Experiment
GRAPE	Global Retrieval of ATSR cloud Parameters and Evaluation
GSICS	Global Space-based Inter-Calibration System
GTS	Global Telecommunication System
IPCC	International Panel on Climate Change
IR	Infrared
JAXA	Japan Aerospace Exploration Agency
K	Kelvin
MODIS	Moderate Resolution Imaging Spectroradiometer
MSG	Meteosat Second Generation
MTG	Meteosat Third Generation
NASA	National Aeronautics and Space Administration
NERC	Natural Environment Research Council
CEDA	NERC Earth Observation Data Centre
NetCDF	Network Common Data Form

NIR	Near Infrared
NOAA	National Oceanic & Atmospheric Administration
NSIDC	National Snow and Ice Data Center
NWP	Numerical Weather Prediction
OE	Optimal Estimation
OLR	Outgoing Longwave Radiation
ORAC	Oxford RAL Aerosol and Cloud
UO	University of Oxford
PUG	Product User Guide
PVP	Product Validation Plan
PVIR	Product Validation and Intercomparison Report
RAL	Rutherford Appleton Laboratory
RTM	Radiative Transfer Model
RTTOV	Radiative Transfer for TOVS
SAF	Satellite Application Facility
SCOPE-CM	Sustained and Coordinated Processing of Environmental Satellite Data for Climate Monitoring
SEVIRI	Spinning Enhanced Visible and Infrared Imager
SLSTR	Sea and Land Surface Temperature Radiometer
SOW	Statement Of Work
SST	Sea Surface temperature
SVR	System verification Report
TCDR	Thematic Climate Data Record
TIR	Thermal Infrared
TR	Technical Requirement
WCRP	World Climate Research Program
WMO	World Meteorology Organisation

	Doc:		Cloud_cci+_D4.1_PVIR_v3.0.docx		
	Date:		20.11.2023		
	Issue:	3	Revision:	0	Page 52

## 6 References

- ADPv3.0**, Algorithm Development Plan ESA Cloud\_cci+, Issue: 3 Revision: 0, Released: tbd
- ATBDv9.0**, Algorithm Theoretical Baseline Document (ATBD) - ESA Cloud\_cci+, Issue:9, Revision: 0, Released: 20.11.2023, available at <https://climate.esa.int/en/projects/cloud/>
- Chepfer, H., Bony, S., Winker, D., Cesana, G., Dufresne, J. L., Minnis, P., ... & Zeng, S. (2010)**. The GCM-oriented calipso cloud product (CALIPSO-GOCCP). *Journal of Geophysical Research: Atmospheres*, 115(D4).
- Delanoë, J., and R. J. Hogan, 2008**: A variational scheme for retrieving ice cloud properties from combined radar, lidar, and infrared radiometer, *J. Geophys. Res.*, 113, D07204, doi:10.1029/2007JD009000.
- Delanoë, J., and R. J. Hogan, 2010**: Combined CloudSat-CALIPSO-MODIS retrievals of the properties of ice clouds. *J. Geophys. Res.*, 115, D00H29, doi:10.1029/2009JD012346.
- Doelling, D. R., Loeb, N. G., Keyes, D. F., Nordeen, M. L., Morstad, D., Nguyen, C., Wielicki, B. A., Young, D. F. and M. Sun, 2013**: Geostationary enhanced temporal interpolation for CERES flux products. *J. Atmos. Oceanic Technol.*, 30: 1072-1090.
- Driemel, A., Augustine, J., Behrens, K., Colle, S., Cox, C., Cuevas-Agulló, E., Denn, F. M., Duprat, T., Fukuda, M., Grobe, H., Haeffelin, M., Hodges, G., Hyett, N., Ijima, O., Kallis, A., Knap, W., Kustov, V., Long, C. N., Longenecker, D., Lupi, A., Maturilli, M., Mimouni, M., Ntsangwane, L., Ogihara, H., Olano, X., Olefs, M., Omori, M., Passamani, L., Pereira, E. B., Schmithüsen, H., Schumacher, S., Sieger, R., Tamlyn, J., Vogt, R., Vuilleumier, L., Xia, X., Ohmura, A., and König-Langlo, G, 2018**: Baseline Surface Radiation Network (BSRN): structure and data description (1992-2017), *Earth Syst. Sci. Data*, 10: 1491-1501, doi:10.5194/essd-10-1491-2018
- Karlsson, K. -G. & E. Johansson (2013)**: On the optimal method for evaluating cloud products from passive satellite imagery using CALIPSO-CALIOP data: example investigating the CM SAF CLARA-A1 dataset. *Atm. Meas. Tech.*, 6, 1271-1286, <http://dx.doi.org/10.5194/amt-6-1271-2013>
- Kato, S., Rose, F. G., Rutan, D. A., Thorsen, T. E., Loeb, N. G. Doelling, D. R., Huang, X., Smith, W. L., Su, W. and S.-H. Ham, 2018**: Surface irradiances of Edition 4.0 Clouds and the Earth's Radiant Energy System (CERES) Energy Balanced and Filled (EBAF) data product, *J. Climate*, 31: 4501-4527.
- Kummerow, C., R. Ferraro, and D. Randel. 2020**. AMSR-E/AMSR2 Unified L2B Global Swath Surface Precipitation, Version 1. [AU\_Rain]. Boulder, Colorado USA. NASA National Snow and Ice Data Center Distributed Active Archive Center. doi: <https://doi.org/10.5067/P5MCTDH7674A.06/10/2021>.
- Loeb, N. G., Priestley, K. J., Kratz, D. P., Geier, E. B., Green, R. N., Wielicki, B. A., Hinton, P. O. R. and S. K. Nolan, 2001**: Determination of unfiltered radiances from the Clouds and the Earth's Radiant Energy System (CERES) instrument. *J. Appl. Meteor.*, 40: 822-835.
- Loeb, N. G., Wielicki, B. A., Doelling, D. R., Smith, G. L., Keyes, D. F., Kato, S., Manalo-Smith, N. and T. Wong, 2009**: Toward optimal closure of the Earth's top-of-atmosphere radiation budget, *J. Climate*, 22: 748-756. Doi: <https://doi.org/10.1175/2008JCLI2637.1>.
- Loeb, N. G., Doelling, D. R., Wang, H., Su, W., Nguyen, C., Corbett, J. G., Liang, L., Mitrescu, C., Rose, F. G., and S. Kato, 2018**: Clouds and the Earth's Radiant Energy System (CERES) Energy Balanced and Filled (EBAF) Top-of-Atmosphere (TOA) Edition-4.0 Data Product. *J. Climate*, 31: 895-918. Doi: [https://doi.org/10.5067/Terra+Aqua/CERES/EBAF-TOA\\_L3B004.0](https://doi.org/10.5067/Terra+Aqua/CERES/EBAF-TOA_L3B004.0).

	<b>Doc:</b>		Cloud_cci+_D4.1_PVIR_v3.0.docx		
	<b>Date:</b>		20.11.2023		
	<b>Issue:</b>	3	<b>Revision:</b>	0	Page 53

**NASA/LARC/SD/ASDC (a).** (2019). CERES Energy Balanced and Filled (EBAF) TOA Monthly means data in netCDF Edition4.1 [Data set]. NASA Langley Atmospheric Science Data Center DAAC. Retrieved from [https://doi.org/10.5067/TERRA-AQUA/CERES/EBAF-TOA\\_L3B004.1](https://doi.org/10.5067/TERRA-AQUA/CERES/EBAF-TOA_L3B004.1)

**NASA/LARC/SD/ASDC (b).** (2019). CERES Energy Balanced and Filled (EBAF) TOA and Surface Monthly means data in netCDF Edition 4.1 [Data set]. NASA Langley Atmospheric Science Data Center DAAC. Retrieved from [https://doi.org/10.5067/TERRA-AQUA/CERES/EBAF\\_L3B.004.1](https://doi.org/10.5067/TERRA-AQUA/CERES/EBAF_L3B.004.1)

**Rossow, W. B., & Schiffer, R. A.** (1999). Advances in understanding clouds from ISCCP. Bulletin of the American Meteorological Society, 80(11), 2261-2288.

Sheethala, C., and Á. Horváth (2010), Global assessment of AMSR-E and MODIS cloud liquid water path retrievals in warm oceanic clouds, J. Geophys. Res., 115, D13202, doi:10.1029/2009JD012662.

**Su, W., Corbett, J., Eitzen, Z. and L. Liang,** 2015: Next-generation angular distribution models for top-of-atmosphere radiative flux calculation from CERES instruments: methodology. Atmos. Meas. Tech., 8 (2): 611-632. Doi: <http://dx.doi.org/10.5194/amt-8-611-2015>.

**Stengel, M., Stapelberg, S., Schlundt, C., Karlsson, K.-G., Meirink, J.F., Poulsen, C., Bojanowski, J., and Stöckli, R.:** Cloud\_cci Product validation and Intercomparison Report, (2020) [http://www.esa-cloud-cci.org/sites/default/files/upload/Cloud\\_cci\\_D4.1\\_PVIR\\_v6.1.pdf](http://www.esa-cloud-cci.org/sites/default/files/upload/Cloud_cci_D4.1_PVIR_v6.1.pdf)

**Vaughan, M., Powell, K., Kuehn, R., Young, S., Winker, D., Hostetler, C., Hunt, W., Liu, Z., McGill, M., and Getzewich, B.,** 2009: Fully Automated Detection of Cloud and Aerosol Layers in the CALIPSO Lidar Measurements, J. Atmos. Oceanic Technol., 26, 2034-2050, doi: 10.1175/2009JTECHA1228.1.

**Wielicki, B. A., Barkstrom, B. R., Harrison, E. F., Lee III, R. B., Smith, G. L. and J. E. Cooper,** 1996: Clouds and the Earth's Radiant Energy System (CERES): An Earth Observing System Experiment, Bull. Amer. Meteor. Soc., 77: 853-868.

**Winker, D. M., Vaughan, M.A., Omar, A., Hu, Y, Powell, K.A., Liu, Z., Hunt, W.H., and Young, S.A.,** 2009: Overview of the CALIPSO mission and CALIOP data processing algorithms, J. Atmos. Oceanic. Technol., 26, 2310-2323, doi:10.1175/2009JTECHA1281.1.

## Annex A - Datasets for comparisons with Cloud\_cci products

### A.1 CALIPSO-CALIOP

Measurements from space-born active instruments (radar + lidar) provide probably the most accurate information we can get about cloud presence in the atmosphere. The reason is the fact that the measured reflected radiation comes almost exclusively from cloud and precipitation particles and is therefore not “contaminated” by radiation from other surfaces or atmospheric constituents as is the case for measurements from most passive radiometers. In this validation study we have decided to utilise measurements from the CALIOP lidar instrument carried by the CALIPSO satellite (included in the A-Train series of satellites - Figure A-1).

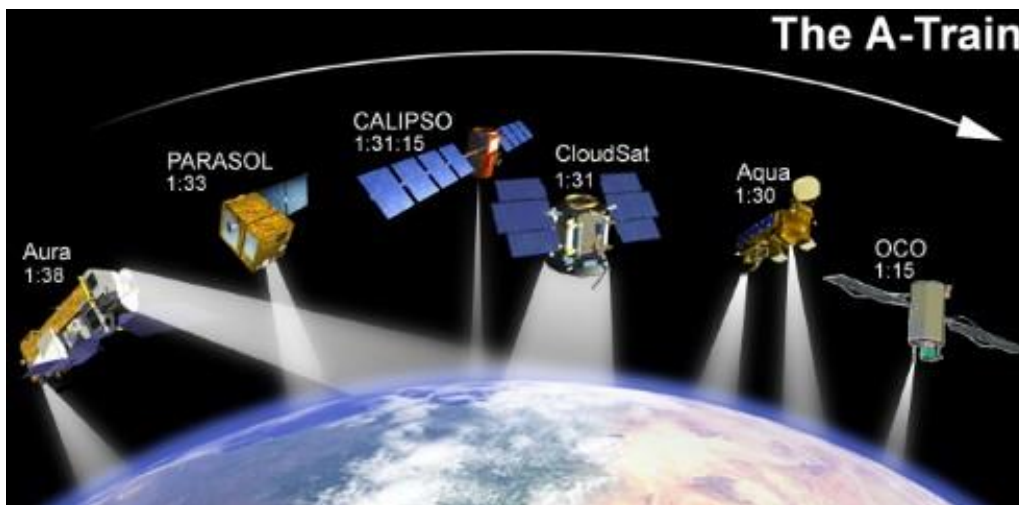


Figure A-0-1 The Aqua-Train satellites. (Image credit: NASA)

The Cloud-Aerosol Lidar and Infrared Pathfinder Satellite Observation (CALIPSO) satellite was launched in April 2006 together with CloudSat. The satellite carries the Cloud-Aerosol Lidar with Orthogonal Polarization (CALIOP) and the first data became available in August 2006 (Winker et al., 2009). CALIOP provides detailed profile information about cloud and aerosol particles and corresponding physical parameters (Vaughan et al., 2009).

CALIOP measures the backscatter intensity at 1064 nm while two other channels measure the orthogonally polarized components of the backscattered signal at 532 nm. The CALIOP cloud product we have used report observed cloud layers i.e., all layers observed until signal becomes too attenuated. In practice the instrument can only probe the full geometrical depth of a cloud if the total optical thickness is not larger than a certain threshold (somewhere in the range 3-5). For optically thicker clouds only the upper portion of the cloud will be sensed. The horizontal resolution of each single FOV is 333 m and the vertical resolution is 30-60 m.

The CALIOP products are available in five different versions with respect to the along-track resolution ranging from 333 m (individual footprint resolution), 1 km, 5 km, 20 km and 80 km. The four latter resolutions are consequently constructed from several original footprints/FOVs. This allows a higher confidence in the correct detection and identification of cloud and aerosol layers compared to when using the original high resolution profiles. For example, the identification of very thin Cirrus clouds is more reliable in the 5 km data record than in the 1 km data record since signal-to-noise levels can be raised by using a combined data record of several original profiles.

We used the CALIOP level-2 5 km cloud layer data record versions 4 (CALIPSO Science Team, 2015) for the validation purpose. The CALIOP cloud layer product reports up to 10 cloud layers per column and provides information about cloud phase and cloud type of each layer as well as

the pressure, height and temperature at each layer’s top. The CALIOP data record classifies cloud layers into cloud types according to Table A-1. To be noticed here is that the ISCCP cloud type method has been used in the sense that the vertical separation of Low (categories 0-3), Medium (categories 4-5) and High (categories 6-7) clouds is defined by use of vertical pressure levels of 680 hPa and 440 hPa.

**Table A-1** *Cloud type categories according to the CALIOP Vertical Feature Mask product.*

Category 0	Low, overcast, thin (transparent St, StCu, and fog)
Category 1	Low, overcast, thick (opaque St, StCu, and fog)
Category 2	Transition stratocumulus
Category 3	Low, broken (trade Cu and shallow Cu)
Category 4	Altostratus ( transparent)
Category 5	Altostratus (opaque, As, Ns, Ac)
Category 6	Cirrus (transparent)
Category 7	Deep convective (opaque As, Cb, Ns)

We only give a quite general description of the CALIPSO data records in this section. It should be emphasized that the CALIOP measurement is probing the atmosphere very efficiently in the along-track direction since it is a nadir pointing instrument. Here, cloud dimensions down to the original FOV resolution (333 m) will be detected. However, it should be made clear that the across-track extension of the observation is still limited to 333 m. Thus, to compare CALIOP-derived results with the results of 3 km SEVIRI pixel data is not entirely consistent (i.e., CALIOP is only capable of covering the SEVIRI pixel properly in one direction and not in the perpendicular direction). However, we believe that this deficiency is of marginal importance. Most cloud systems on the SEVIRI pixel scale will be detected, e.g., it is very unlikely to imagine elongated clouds with size and shapes below 0.3x3 km that might risk remaining undetected within a SEVIRI pixel that coincides with a CALIOP measurement. Most clouds will have aspect ratios for the two horizontal directions that guarantee detection by CALIOP. However, it is also clear that in situations with scattered (sub-pixel) cloudiness within the SEVIRI pixel, some optically thick clouds may be detected by the SEVIRI cloud detection while not being covered at all by CALIOP FOVs. Thus, some small bias between SEVIRI and CALIOP observations due to this effect appears unavoidable. It is important to consider that the CALIOP lidar instrument is much more sensitive to cloud particles than the measurement from a passively imaging instrument. It means that a significant fraction of all CALIOP detected clouds will not be detected from imagers. This sensitivity difference also propagates into CPH and CTH, which will typically be sensed at a lower cloud layer by passive instruments compared to CALIOP. Thus, to get reasonable and justified results one should theoretically consider filtering out the contributions from the very thinnest clouds. We have applied this approach in this validation study, both in the study of cloud amounts (CFC) and cloud top heights (CTO).

The cloud detection efficiency with CALIOP is slightly different day and night because of the additional noise from reflected solar radiation at daytime that can contaminate lidar backscatter measurements. However, [Chepfer et al. \(2010\)](#) reports that this can introduce an artificial difference of not more than 1 % when comparing night time and daytime data.

In conclusion: Despite the fact that the CALIPSO cloud observations most likely are the best available cloud reference data record being released so far, we might still see a negative bias of a few percentage points in cloud cover when using exclusively the 5 km data record. Other errors, e.g. due to mis-interpretation of heavy aerosol loads as clouds, are in this respect of minor importance when judging the effect on full global orbits.

## A.2 AMSR2

Passive microwave imagers, such as the Advanced Microwave Scanning Radiometer 2 (AMSR2) onboard the polar orbiting Global Change Observation Mission 1st-Water (GCOM-W1) satellite,

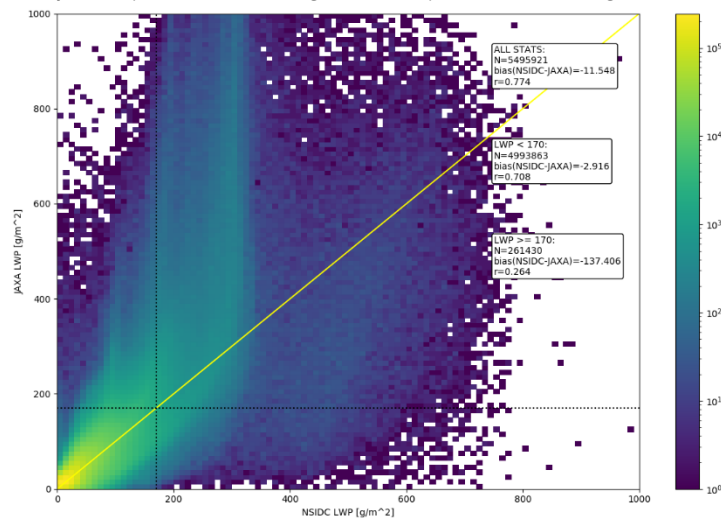
can be used to retrieve column-integrated liquid water. AMSR2 onboard GCOM-W1 is the successor of AMSR-E onboard Aqua and is as CALIPSO and Aqua also in the A-Train orbit.

AMSR2 is a dual-polarization conical-scanning passive microwave radiometer with a total of 16 channels ranging from 6.9 to 89 GHz. This instrument was designed to measure cloud properties, sea surface temperature and surface water, ice and snow. Because the microwave (MW) channels usually fully penetrate clouds, they provide a direct measurement of the total liquid (but not solid) cloud condensate amount. For precipitating clouds an estimate of the rain water path has to be made and subtracted from the total liquid water path to retrieve the cloud liquid water path. AMSR2 data are in this document used for Level-2 validation of LWP.


For this validation the National Snow and Ice Data Center (NSIDC) “AMSR-E/AMSR2 Unified L2B Global Swath Surface Precipitation, Version 1 (AU\_Rain)” product is used (Kummerow et al., 2020). The data were generated using the Goddard Profiling Algorithm. AU\_Rain uses the Japan Aerospace Exploration Agency (JAXA) AMSR2 Level-1R input brightness temperatures ([https://suzaku.eorc.jaxa.jp/GCOM\\_W/data/data\\_w\\_use.html](https://suzaku.eorc.jaxa.jp/GCOM_W/data/data_w_use.html)).

JAXA itself has also an LWP L2 product based on AMSR2 ([https://suzaku.eorc.jaxa.jp/GCOM\\_W/data/data\\_w\\_index.html](https://suzaku.eorc.jaxa.jp/GCOM_W/data/data_w_index.html)). We decided to use the NSIDC product but we also investigated the difference between the two datasets. As the NSIDC data are higher resolved in along scan direction (392 vs. 243 pixels) we resampled the NSIDC data to the lower resolution JAXA grid for comparison. Figure A-1 shows a scatter plot of NSIDC vs. JAXA AMSR2 LWP. For the LWP range we are interested in ( $< 170 \text{ g/m}^2$ ), NSIDC LWP is on average about  $3 \text{ g/m}^2$  lower than JAXA. For  $\text{LWP} > 170 \text{ g/m}^2$  the both products significantly diverge. In this regime JAXA LWP is much higher than NSIDC.

**Figure A-1** This figure shows a scatter plot of JAXA AMSR2 L2 LWP (y-axis) vs. NSIDC AMSR2 L2 LWP (x-axis). The yellow line is the 1:1 line. The colorbar has a logarithmic scale. The dashed lines are marking the  $170 \text{ g/m}^2$  thresholds of both datasets. The three boxes show statistics for all data pairs, for  $\text{LWP} < 170 \text{ g/m}^2$  and for  $\text{LWP} > 170 \text{ g/m}^2$ .





	Doc:		Cloud_cci+_D4.1_PVIR_v3.0.docx		
	Date:		20.11.2023		
	Issue:	3	Revision:	0	Page 57

### A.3 DARDAR

DARDAR (raDAR/liDAR) is a combined product based on measurement by CALIOP lidar and CPR onboard CloudSat. CPR is a nadir-looking cloud profiling radar sensing the atmosphere from above at 94 GHz. The instrument's sensitivity is defined by a minimum detectable reflectivity factor of -30 dBZ and calibration accuracy of 1.5 dB. The minimum detectable reflectivity factor requirement was reduced to -26 dBZ when the mission was changed to put CloudSat into a higher orbit for formation flying in A-train. The DARDAR dataset (Delanoë and Hogan, 2008,2010) provides the result from a synergistic variational retrieval method combining the measurements from the CALIOP lidar, the CLOUDSAT radar and the MODIS imager, all three elements of the A-Train satellite constellation. By combining these different measurements, consistent profiles of microphysical properties are retrieved based on the specific particle size (instrumental) wavelength sensitivities. The lidar signals for instance are sensitive to the particle surfaces in the line of sight ( $\sim$ radius<sup>2</sup>), which is dominated by the smaller particles in a particle size distribution (PSD) whereas the radar signals are sensitive to the square of the particle volume which is dominated by the larger particles in the PSD. When both signals are available the combined PSD sensitivities provide the best guess of extinction, effective particle radius and IWC. When only one of the signals is available, i.e. when the lidar is fully attenuated or when the particles are too small to be detected by radar, the DARDAR retrievals are based on the single instrument parameterizations. The optimal estimation framework used for this retrieval ensures a smooth transition from these different regimes. The DARDAR product has the CALIPSO vertical resolution of 60m and the CloudSat horizontal resolution of 1.4km.

The DARDAR-cloud dataset in version 3.00 for the current evaluation has been downloaded from the ICARE site:

<https://www.icare.univ-lille.fr/dardar/overview-dardar-cloud/>

DARDAR is used for level-2 evaluation of IWP. Important to note, DARDAR is much more sensitive to thin ice cloud than passive imagers. In the lower part of the atmosphere, the reflectance of the surface affects the backscattered radar signal, so clouds may not be properly detected below 1 km distance to the surface.


## A.4 BSRN: Baseline Surface Radiation Network

The international Baseline Surface Radiation Network (BSRN) provides ground-level radiation measurements with high temporal resolution for the validation of satellite data, the validation and improvement of radiative transfer calculations in climate models as well as the detection and monitoring of long-term changes in surface radiation fluxes (Driemel et al., 2018). The BSRN started working in 1992 with 9 stations and currently comprises a network of 46 active stations (status 2021-12-07), which are distributed over all continents and oceanic environments. The stations deliver data to the archive called the World Radiation Monitoring Center (WRMC), which is hosted at the Alfred Wegener Institute (AWI) in Bremerhaven, Germany. The data is freely available at <https://bsrn.awi.de/data/data-retrieval-via-pangaea>

BSRN stations measure direct, diffuse and global downwelling shortwave and longwave fluxes in 1 min temporal resolution. The manned stations are located at positions, which are representative of a relatively large surrounding area for the use in satellite and climate model validation. The quality controlled datasets are available for the years 1992 to 2021 in ASCII file format. In this work we used specially calculated monthly means of daily mean products:

- Global shortwave radiation (SWD)
- Long-wave downward radiation (LWD)
- Shortwave upward radiation (SWU)
- Long-wave upward radiation (LWU)



	Doc:		Cloud_cci+_D4.1_PVIR_v3.0.docx		
	Date:		20.11.2023		
	Issue:	3	Revision:	0	Page 59


## A.5 SYNOP: manual cloud observations from surface stations

Observations of total cloud cover made at meteorological surface stations (i.e. synoptic observations - hereafter called SYNOP) constitute one of the data records used to evaluate the cloud fractional coverage estimates. The SYNOP data used is from the local DWD archive of collected global SYNOP reports following the guidance of the *Guide to Meteorological Instruments and Methods of Observations* (WMO, 2008).

At manned stations the total cloud cover is visually estimated by human observers, at automated stations in contrast ceilometers are used for that purpose. For data quality reasons, only those SYNOP reports provided by manned airport stations were taken into account (~1800 stations globally). SYNOP total cloud cover observations are used for the evaluation of level-3 cloud cover estimates. Manual cloud observations are affected by many sources of error. We list some of the most important in the following:

- The observation is subjective in nature, i.e., despite clear instructions on how to make an observation, differences will appear because of different interpretations from person to person. This introduces a random noise in global cloud amount observations but may also lead to geographical biases (reflecting some systematic behaviour related to the way people have been educated/trained).
- The human eye has a detection limit for when a cloud can be clearly discernible against a cloud-free sky. This limit is somewhere in the cloud optical thickness range of 0.5-1.0 (with some dependence on solar zenith angle and on which viewing angles clouds are observed and the degree of aerosol load or haze in the troposphere). Thus, many satellite sensors have a higher sensitivity to e.g. cirrus detection than SYNOP observations.
- At night, the random error in the observations increases, naturally since the observer does not have a clear sky background against which a cloud can be observed (i.e., clouds are as dark as the cloud-free sky). However, accuracies improve in the presence of moonlight. Nevertheless, the overall effect is normally a negative bias (underestimated cloud amounts) since the observer is tempted to report cloud free conditions as soon as stars become visible, thus neglecting that large fractions of thin cirrus and other cloud types may still be present.
- A well-known deficiency of SYNOP observations is the scenery effect, i.e. overestimation of convective cloud towers at a slanted view (Karlsson, 2003). This effect is thus most pronounced in the summer season and for low to moderate cloud amounts when the overestimation easily can reach values of 20-30 % (1-2 octas).
- It is important to consider that most SYNOP stations are located at land stations and with higher density in developed countries. Thus, global averages tend to be biased towards land conditions in densely populated countries.

Since no rigorous study has been able to cover all those aspects in a quantitative manner (mainly because of lack of an absolute truth as reference) we can only make a very general qualitative statement about the overall quality. We would suggest that the accuracy of SYNOP observations vary between approximately +10 % (some overestimation) at daytime conditions changing to -10 % or worse (some underestimation) at night time. However, the variability (precision) probably reaches higher absolute values and it is largest during night conditions. This may lead to a strong seasonal variation with the worst accuracy and precision features during the winter season (at least at middle and high latitudes including the polar regions). It is worth noting that the increasing trend to replace manual cloud observations with automatic observations from ceilometers will change the accuracy and precision of cloud observations in several ways. Despite their subjective character and varying quality, SYNOP observations still provide a useful reference data set suitable for monitoring and validating space-based estimations of cloud coverage, especially due to their long-term availability.

	Doc:		Cloud_cci+_D4.1_PVIR_v3.0.docx		
	Date:		20.11.2023		
	Issue:	3	Revision:	0	Page 60

## A.6 CERES: Cloud and the Earth’s Radiant Energy System

The Cloud and the Earth’s Radiant Energy System (CERES) Energy Balanced and Filled (EBAF) top-of-atmosphere (TOA) Edition 4.1 (Ed.4.1) data product (CERES\_EBAF-TOA\_Edition4.1) provides long-term shortwave (SW) and longwave (LW) TOA fluxes for all- and clear-sky conditions (NASA/LARC/SD/ASDC (2019a)). The CERES instruments fly on the *Terra* and *Aqua* satellites and cover a period from March 2000 to June 2002 for Terra only, and cover combined Terra and Aqua observations from July 2002 to 2021. Each instrument measures filtered radiances in the shortwave wavelengths between 0.3 and 5  $\mu\text{m}$ , total wavelengths between 0.3 and 200  $\mu\text{m}$  and window wavelengths between 8 and 12  $\mu\text{m}$ . The filtered radiances are converted to unfiltered SW, LW and window radiances following Loeb et al. (2001), which in turn are converted to instantaneous TOA radiative fluxes using empirical angular distribution models (Su et al., 2015). The CERES instruments provide global coverage daily, and monthly mean regional fluxes are based upon daily samples over the entire globe.

However, the standard CERES data products are produced using coincident imager data from the Moderate Resolution Imaging Spectrometer (MODIS) and the Visible Infrared Imaging Radiometer Suite (VIIRS). To provide a diurnally complete representation of Earth’s radiation budget, all available geostationary imager data between 60°S and 60°N are also used to account for cloud radiation changes between CERES observation times. A specialty about the CERES EBAF product is the adjustment of occurring radiation imbalances within the CERES-based Earth Radiation Budget (ERB). Therefore an objective algorithm is applied to adjust SW and LW TOA fluxes within their ranges of uncertainty to remove the inconsistency between average global net TOA flux and heat storage in the earth-atmosphere system (Loeb et al. 2009).

For intercomparison we used the CERES\_EBAF-TOA\_Edition4.1 longwave and shortwave monthly mean fluxes for all-sky conditions. In CERES EBAF Ed4.1, the monthly mean fluxes are determined by spatially averaging the instantaneous TOA flux values on a 1°x1° grid, temporally interpolating between observed values at 1-h increments for each GMT hour of every month and then averaging all hour boxes in month (Doelling et al. 2013). The used products are summarized as follows:

- Top of the Atmosphere Longwave Flux, Monthly Means, All-Sky conditions
- Top of the Atmosphere Shortwave Flux, Monthly Means, All-Sky conditions


In addition to the TOA fluxes, we also used the CERES\_EBAF\_Edition4.1 product (NASA/LARC/SD/ASDC (2019b)) containing the surface fluxes (successor of Ed4.0 EBAF-Surface). Surface fluxes in CERES\_EBAF\_Edition4.1 are derived from the CERES data products: (i) CERES SYN1deg-Month Ed4.1 provides computed surface fluxes to be adjusted, (ii) CERES EBAF-TOA Ed4.1 provides the CERES-derived TOA flux constraints by observations and (iii) SYN1deg-Hour provides weights to compute monthly mean computed clear-sky TOA fluxes. The monthly mean all-sky surface shortwave and longwave fluxes for 1° x1° grids are computed by averaging hourly CERES SYN1deg Ed4.1 all-sky fluxes (Wielicki et al., 1996).

In order to minimize the error in surface fluxes due to uncertainties in the input data sources, the CERES\_EBAF\_Edition4.1 data product introduces several additional constraints based upon information from other independent data sources, such as CERES TOA fluxes, Atmospheric Infrared Sounder (AIRS) derived temperature and humidity profiles as well as CALIPSO/CloudSat-derived vertical profiles of clouds. With the help of Goddard Earth Observing System (GEOS) atmospheric profiles and CERES-derived surface albedo radiative transfer model calculations can be applied. From CERES\_EBAF\_Edition4.1 Surface fluxes we used the following products:

- Surface Shortwave Flux Down, Monthly Mean, All-Sky conditions
- Surface Longwave Flux Down, Monthly Mean, All-Sky conditions

The CERES\_EBAF-TOA\_Edition4.1 is freely available at:  
[https://doi.org/10.5067/TERRA-AQUA/CERES/EBAF-TOA\\_L3B004.1](https://doi.org/10.5067/TERRA-AQUA/CERES/EBAF-TOA_L3B004.1)

The CERES\_EBAF\_Edition4.1 is freely available at:  
[https://doi.org/10.5067/TERRA-AQUA/CERES/EBAF\\_L3B.004.1](https://doi.org/10.5067/TERRA-AQUA/CERES/EBAF_L3B.004.1)

	<b>Doc:</b>		Cloud_cci+_D4.1_PVIR_v3.0.docx		
	<b>Date:</b>		20.11.2023		
	<b>Issue:</b>	3	<b>Revision:</b>	0	Page 61

### A.7 CLAAS-3: CLOUD property dAtAset using SEVIRI

The Climate Monitoring Satellite Application Facility (CMSAF) CLOUD property dAtAset using SEVIRI in version 3 (CLAAS-3) monthly means are used to compare the monthly mean Cloud\_cci+ Level-3C data to another SEVIRI-based Climate Data Record (CDR).